PROPAGATION OF TRANSIENT STRESSES ACROSS NONCOHESIVE OBLIQUE INTERFACES

By

Ulrich Lorber

A thesis submitted to the Faculty and the Board of Trustees of the Colorado School of Mines in partial fulfillment of the requirements for the degree of Master of Science in Mining Engineering.

Signed: U Lorber
Ulrich Lorber

Golden, Colorado

Date: 10 October, 1961

Approved: ______________
John S. Rinehart
Thesis Advisor

____
Lute J. Parkinson
Head of Department

Golden, Colorado

Date: ______________, 1961

ABSTRACT

In this study of the propagation of transient compressive stresses across noncohesive oblique interfaces, the experimental setup consists of a Plexiglas specimen cut into two parts, the contacting surfaces being polished to a high degree. Specimens of several different shapes are used. The interfaces form predetermined angles with the normal to the wave's path. These angles range between 0° and 75°. An electric detonator attached to one side of the specimen provides the stress pulse, which at a distance of 2 in. has a maximum stress of approximately 6000 lb/in.^{2} and a duration of about 3 μsec. A small circular pellet of Plexiglas is placed on the side opposite to the detonator. The velocity at which the pellet flies off is a measure of the impulse trapped in it. The impulse per unit area, in turn, is determined by the integral $\int \sigma \, dt$, thus providing a means to compute the stress-time function.

By plotting the average relative stress against the angle of the interface, one can draw the following conclusions: for interfaces of up to 45° (0° interface is perpendicular to wave path), the curve follows

very closely a theoretical curve; the curve has a minimum between 60° and 70°, followed by a sharp rise with increasing angle of the interface. Because of practical difficulties, no tests were run for interface angles of more than 75°.

Through a mathematical approach, and by applying the adequate boundary conditions for this type of interface, one can obtain a trigonometric relationship for the displacement amplitudes. Although this equation follows the trend of the experimental curve, the effect of the interface angle appears to be less marked than that observed in the experimental curve.

The applications of this investigation in the field of mining engineering appear to be multiple. The design of efficient blasting methods in large open pit mines, for example, presupposes a good understanding of the process of rock breakage. Rock breakage, in turn, is certainly affected by the mode of propagation of the stress pulses across the rock itself. In many cases, the cracks and fissures in the rock can be considered basically as noncohesive interfaces. The location and design of underground openings for defense also requires the study of wave propagation across strata and particularly across geological features in the earth's crust.

CONTENTS

Page

APPENDICES

ILLUSTRATIONS

ACKNOWLEDGMENTS

The author wishes to express his sincere appreciation to the following persons and organizations:

Dr. John S. Rinehart, Director of the Mining Research Laboratory, Colorado School of Mines, for his guidance and assistance in the investigation and the preparation of this thesis.

Professor Albert L. Gosman, Professor Raymond R. Gutzman, and Dr. John J. Reed, for their interest in the work and their suggestions.

The National Science Foundation, for providing the funds necessary to carry out this investigation.

The Anaconda Company, for providing the initial scholarship which enabled the author to come to the United States.

INTRODUCTION

The work presented in this thesis forms part of an extensive research program studying the propagation of transient stresses under a variety of specific conditions. This program -- supported in part by the National Science Foundation -- is being conducted at the Mining Research Laboratory of the Department of Mining Engineering, Colorado School of Mines, under the guidance of Dr. John S. Rinehart.

This thesis covers the phenomena involved in the propagation of transient stresses across noncohesive, oblique interfaces. The main purpose has been to find, by experimental means, a relationship which expresses the pulse amplitude as a function of the interface angle. For several reasons -- accuracy as well as simplicity -- the average relative stress rather than the maximum stress has been chosen to represent the pulse amplitude.

Although this problem is basic in wave propagation, the previous work in this subject is rather inextensive. On the other hand, a mathematical solution for a more general but similar problem has already been worked out.

This research work has ample and practical value in different fields. In first term, a strictly physical problem is involved -- the propagation of transient stresses across noncohesive, oblique interfaces. The geophysicist, as well as the seismologist, has a definite interest in these phenomena. They both have to deal with faults and fissures in the earth's crust, which in many instances can be considered basically as noncohesive interfaces. In mining engineering and particularly in the field of blasting, a more efficient use of explosives requires a better understanding of the basic principles involved in the process. And here again, certainly, the propagation of stresses across cracks in the rock must play a major role.

SYMBOLS AND UNITS

Unless otherwise stated in a particular chapter, the following symbols are used throughout this thesis:

A	area
c	velocity of propagation, in general
c_l	velocity of longitudinal waves
c_t	velocity of transverse waves
E	modulus of elasticity, energy
e	base of naperian logarithms
F	force
I	impulse
i	$\sqrt{-1}$
K	displacement amplitude, in general
k	constant, quotient of c_l/c_t
L	length of pulse
m	mass
p	2π times the frequency

R	coefficient of reflection
r	radius, distance from focus
T	period
t	time
t_p	thickness of pellet
u, v, w	displacements in x, y, and z directions respectively
v	particle velocity
x, y, z	cartesian coordinates
α	angle of incidence
β	angle of reflected shear wave
θ	dilatation
λ, μ	Lamé's constants
ν	Poisson's ratio
ρ	density
σ	stress
σ_{xx}, σ_{xy}	components of stress in cartesian coordinates
τ	shear stress
ϕ	displacement function

The CGS system of units has been adopted, although a considerable number of measurements will be kept in English-system units, for convenience. The CGS system has the following basic units:

	Unit	Abbreviation
length	centimeter	cm
mass	gram	g
time	second	sec

Derived units are

force	dyne	$g\text{-}cm/sec^2$
stress		$dyne/cm^2$
impulse/area		g/cm-sec
velocity		cm/sec

Conversion factors, to change from CGS to English units:

1 cm	0.0328 ft
	0.3937 in.
1 g	$0.002204\ lb_{mass}$
1 dyne	$2.248 \times 10^{-6}\ lb_{force}$
1 g/cm-sec	$0.145 \times 10^{-4}\ lb\text{-}sec/in.^2$
1 $dyne/cm^2$	$0.145 \times 10^{-4}\ lb/in.^2$

BACKGROUND THEORY

In the following chapter, the basic principles involved in this work will be summarized. The physical entities will be defined and discussed. The report "On Fractures caused by Explosions and Impacts" (Rinehart, 1960) is used extensively as a guide, and its use is suggested here for further reference.

In general, a transient stress is a disturbance caused by a load which is applied for a rather short time (see also fig. 1). A transient stress can be produced by a mechanical blow or, as was the case throughout this research work, by a detonating explosive.

We have to distinguish between two different types of stress generated by such an impulsive load: the longitudinal and the transverse waves. In general, both types will be generated simultaneously. For the longitudinal disturbance the particle motion is in the direction of propagation; for the transverse disturbance it is in a plane normal to the direction of propagation of the pulse.

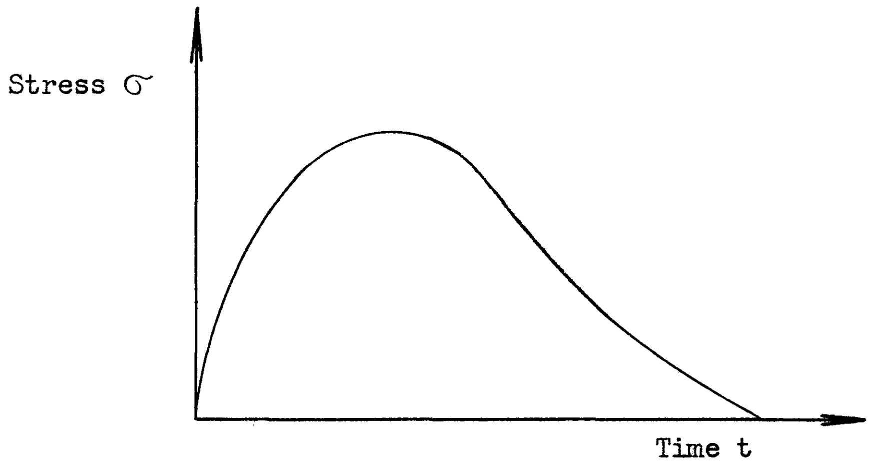

Fig. 1: Stress vs. time curve for a transient pulse

VELOCITIES OF PROPAGATION

A transient disturbance will travel at a certain velocity, depending upon the elastic constants and the density of the material. For the two types of disturbances there are two different velocities of propagation. They are given by the $c_l = \sqrt{\frac{E\ (1-\nu)}{\rho(1+\nu)(1-2\nu)}}$t, 1960, p. 6-7)

$$c_l = \sqrt{\frac{E\ (1-\nu)}{\rho(1+\nu)(1-2\nu)}} \tag{1}$$

and

$$c_t = \sqrt{\frac{E}{2\rho\ (1+\nu)}} \tag{2}$$

where c_l is propagation velocity of longitudinal wave

c_t is propagation velocity of transverse wave

E is modulus of elasticity

ν is Poisson's ratio

ρ is density

(for complete list of symbols see also p. 3-4).

The two formulas can be developed from the general equations of wave motion. Values for c_l and c_t in Plexiglas are given in the appendix.

By applying Newton's second law of motion one can obtain a useful relationship between velocity of propagation and particle velocity. Let us consider fig. 2, in which a longitudinal disturbance is being propagated in a material of cross-sectional area A:

We can write then

$$F\,dt = dm\ v$$

where $$dm = \rho\ A\ dx$$

and v is particle velocity

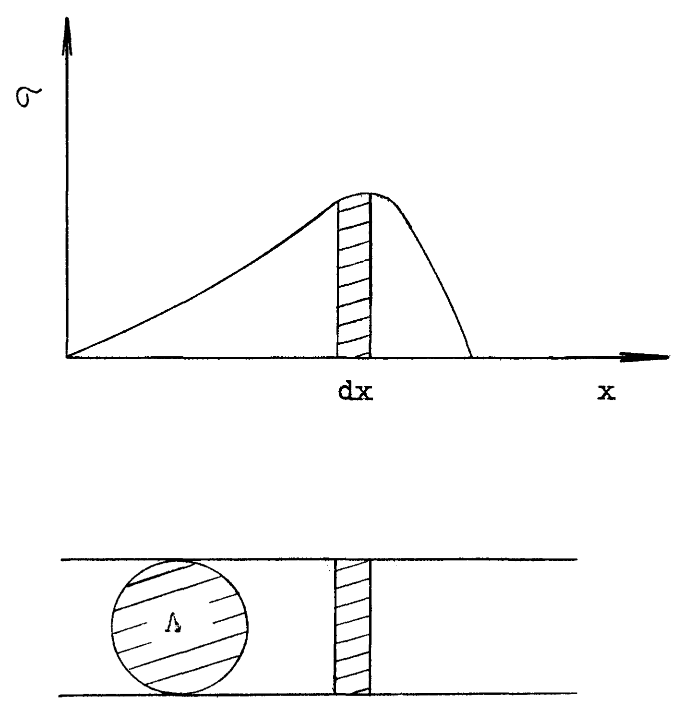

Fig. 2: Pulse propagating in a rod

Replacing and rearranging we obtain

$$\frac{F}{A} = \rho \frac{dx}{dt} v$$

or finally

$$\sigma = \rho c_1 v \tag{3}$$

A similar relation can be obtained for transverse waves.

DIRECTION OF PARTICLE MOTION

For a compression stress wave, the particle velocity and the wave motion are in the same direction. For a tension wave, they are in opposite directions.

EFFECT OF A FREE SURFACE

A stress wave reaching a free surface will be reflected from it. At the surface the normal stress has to be zero.

In general an incident longitudinal stress wave will generate a reflected longitudinal and a reflected transverse wave. For normal incidence, no transverse wave is generated, and the reflected wave is then a mirror image of the incident wave, and opposite in sign. Therefore, a compression pulse is reflected as tension, and vice versa.

The following relations (Rinehart, 1960, p. 9) govern the reflection of a longitudinal stress wave at a free surface:

$$\frac{c_1}{c_t} = \frac{\sin\alpha}{\sin\beta} \tag{4}$$

where α and β are defined in fig. 3.

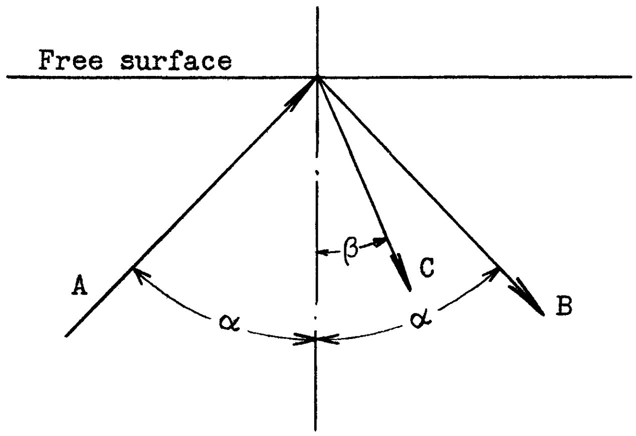

Fig. 3: Reflection at a free surface

$$\sigma_B = -R\ \sigma_A \tag{5}$$

$$\tau_C = (R+1)\ \cot 2\beta\ \sigma_A \tag{6}$$

$$R = \frac{\tan\beta\ \tan^2 2\beta - \tan\alpha}{\tan\beta\ \tan^2 2\beta + \tan\alpha} \tag{7}$$

where R is called the coefficient of reflection.

ENERGY OF A PULSE

The energy of a pulse can be expressed in terms of the stress:

$$E = \int \frac{1}{2}\, dm\ v^2$$

By using eq. 3

$$E = \frac{A}{2\rho c_1^2}\int \sigma^2 dx \tag{8}$$

For a step function with σ = constant

$$E = \frac{A\sigma^2 L}{2\rho c_1^2} = k\sigma^2$$

in which k is a constant factor, dependent upon pulse length.

REFLECTION AND REFRACTION AT AN INTERFACE

When a transient stress disturbance reaches an interface it will be usually both reflected and transmitted (or refracted). In this chapter only normal incidence will be considered. The general case of oblique incidence will be dealt with in detail in the following chapter.

The two following boundary conditions make it possible to calculate the partition of stress at the boundary:

a). The sums of the normal stresses across the interface are equal.

b). The sums of the normal displacements across the interface are equal. This condition can also be applied to the particle velocities.

Put into equations, these conditions are

$$\sigma_I + \sigma_R = \sigma_T$$

$$v_I + v_R = v_T$$

where tensile and compressive stresses are opposite in sign, and I represents the incident pulse; R, the reflected pulse; and T, the transmitted pulse.

With eq. 3 we can express the particle velocities in terms of the stresses, obtaining a system of two equations and three unknowns.

Solving this system for the reflected and transmitted stresses, we finally obtain

$$\sigma_R = \frac{\rho_2 c_2 - \rho_1 c_1}{\rho_2 c_2 + \rho_1 c_1} \sigma_I \tag{9}$$

$$\sigma_T = \frac{2\rho_2 c_2}{\rho_2 c_2 + \rho_1 c_1} \sigma_I \tag{10}$$

From eqs. 9 and 10 it can be seen that when the two media are the same the stress pulse is transmitted completely and no reflection takes place.

PARTICLE VELOCITY

The particle velocity will be discussed in more detail, as it is of basic importance in the experimental technique.

We have seen that, when a stress pulse reaches a free surface, the normal stress at the surface will be zero. At normal incidence, the reflected stress pulse will be equal in magnitude and opposite in sign to the incident pulse. The particle velocity associated with this reflected pulse has the same magnitude and direction as the particle velocity of the incident pulse. It follows that the particle velocity will be doubled at the surface.

The vectorial sum is $\vec{v} - (-\vec{v}) = 2\,\vec{v}$

If small particles were lying on the surface, they would fly off with a velocity equal to twice the instantaneous particle velocity of the pulse. This conclusion can also be obtained by impulse considerations.

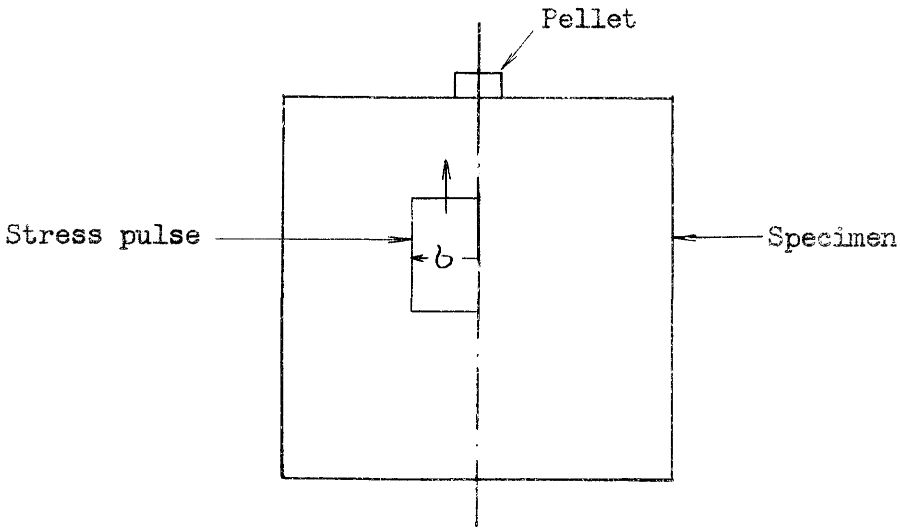

Fig. 4: Transfer of impulse into pellet

Fig. 4 shows a specimen with a thin circular particle -- a pellet -- lying on its flat horizontal surface. Both specimen and pellet are of the same material. A transient compressive stress travelling upwards will reach the interface between specimen and pellet. All the stress will be now transmitted into the pellet and then reflected at its free surface. For simplicity a step function as shown in the figure can be assumed. When the reflected disturbance -- which is a tension pulse -- reaches again the interface, the pellet will fly off. In fact, as soon as the reflected disturbance reaches the interface, the surface of the pellet will start moving away from the specimen, because of the particle velocity associated with the tensile disturbance. Once the pellet separates from the specimen, it will acquire a velocity determined by the trapped impulse.

Computing this impulse by

$$I = \int F \, dt$$

and using Newton's second law

$$I = m\ v \tag{11}$$

the velocity of the pellet is determined as

$$v = \frac{\int F \, dt}{m}$$

which for a square pulse (assuming that the pulse length is greater than twice the pellet thickness) can be written as

$$v = \frac{\sigma A \ 2t_p}{\rho t_p \ A \ c_1}$$

or

$$v = 2\sigma / \rho \ c_1$$

which is equivalent to twice the particle velocity.

In the general case of a stress pulse which is not constant, the velocity is given by

$$\frac{\int_0^{2t_p/c_1} \sigma \, dt}{\rho \ t_p}$$

in which the integral represents the area under the stress-time curve (fig. 5).

INTERFACES

Different types of interfaces can be considered. A first classification is based upon the ability to transmit tensile stresses. In order to transmit tensile stresses, an interface has to have some sort

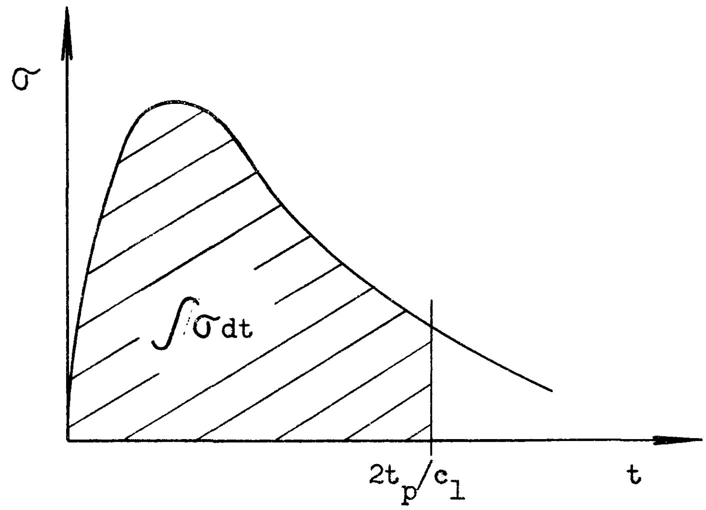

Fig. 5: Area of a stress vs. time curve

of a bonding agent. In general, interfaces will transmit compressive stresses, as these tend to push materials together.

Another classification of interfaces is based upon the ability to transmit shear stresses. A so-called slipping boundary will transmit only stresses normal to it, while slipless boundaries will transmit normal stresses as well as shear stresses parallel to the interface.

A slipping boundary was used in all interface tests of this research work. This was done by applying a thin film of oil to the interface, before putting together both parts of the specimen. As a liquid, the oil will not support the transmission of shear stresses and only normal stresses will cross the interface.

GAPS

A gap is constituted when two materials of an interface are separated by a finite distance. The open space is filled with air, thus showing a quantitative acoustical similarity to a vacuum when compared to a denser material. When a pulse reaches one side of the gap at normal incidence, it will be reflected and the surface set into motion at twice the instantaneous particle velocity. The distance travelled by the free surface is given by

$$s = \int 2v \, dt$$

or

$$s = \frac{2}{\rho c} \int \sigma \, dt$$

in which the integral represents the impulse per unit area of the pulse.

For a certain stress pulse, two types of gaps can be considered: the incomplete gap, in which the moving free surface will eventually reach the opposite side, and the complete gap, where $s <$ gap width d.

DIVERGENCE AND ATTENUATION OF SPHERICAL WAVES

Spherical divergence and attenuation tend to weaken a stress pulse radiating from a point source. Spherical divergence (Rinehart, 1960, p. 115) -- where no energy loss is involved -- can be determined from the relation

$$E_1 A_1 = E_2 A_2 \quad \text{(Conservation of energy)}$$

where E is energy flow per unit area and

A_1 and A_2 represent the areas of two concentric spheres around the point source.

At the same time

$$A_1 \, r_2^2 = A_2 \, r_1^2$$

and therefore

$$\frac{E_1}{E_2} = \frac{r_2^2}{r_1^2} \qquad (12)$$

which means that the energy flow per unit area is inversely proportional to the square of the radius.

From the relation $E = k_1 \sigma^2$

we obtain

$$\sigma = \frac{k_2}{r} \qquad (13)$$

where k_1 and k_2 are constants.

Therefore, the stress at the front of a spherically-diverging pulse is inversely proportional to the radius.

Attenuation involves the loss of a certain amount of the energy of the pulse, which is converted to work done on the material. It is difficult to evaluate the change of the pulse resulting from this effect.

CHANGE IN PROPAGATION VELOCITY

It has been stated before that a longitudinal stress pulse travels with a velocity given by

$$c_1 = \sqrt{\frac{E\,(1-\nu)}{\rho(1+\nu)(1-2\nu)}} \qquad (14)$$

Although this velocity is usually considered to be a constant, this is not quite true. In fact, it can be shown that whereas density and

Poisson's ratio vary within limits which can be considered negligible, Young's modulus will change with stress level. This is evident from a standard stress-strain curve, where E represents the slope of the curve. However, because of the small variation involved, it seems quite difficult to determine the relative change in propagation velocity by such a strain test.

MATHEMATICAL ANALYSIS

The problem undertaken in this research work has been approached in two ways: an experimental one, consisting of several series of tests, and a theoretical one. This chapter is dedicated exclusively to the theoretical approach to the problem.

Macelwane (1936, p. 147-179) describes the reflection and refraction of plane elastic waves in isotropic media. He considers a slipless interface formed by two different materials, which will transmit normal and shear stresses. The method used and described hereafter is an application of Macelwane's method to the particular conditions of this problem.

CONDITIONS

The following two conditions are imposed in the analysis:

1) a slipping interface, formed by a plane between two identical isotropic materials, and
2) a plane elastic longitudinal wave incident on the interface.

In the general case where a longitudinal wave reaches an interface, four new waves will be generated. Therefore, we are concerned with a total of five waves:

1). Incident longitudinal wave

2). Reflected longitudinal wave

3). Reflected transverse wave

4). Refracted longitudinal wave

5). Refracted transverse wave

Fig. 6 shows the vectors of the displacement amplitudes A, C, D, E and F of the five waves.

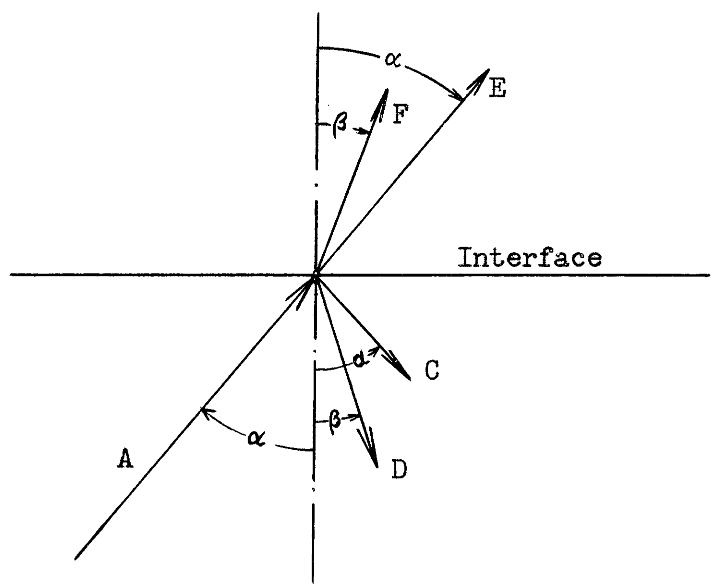

Fig. 6. Amplitude vectors intervening at an interface

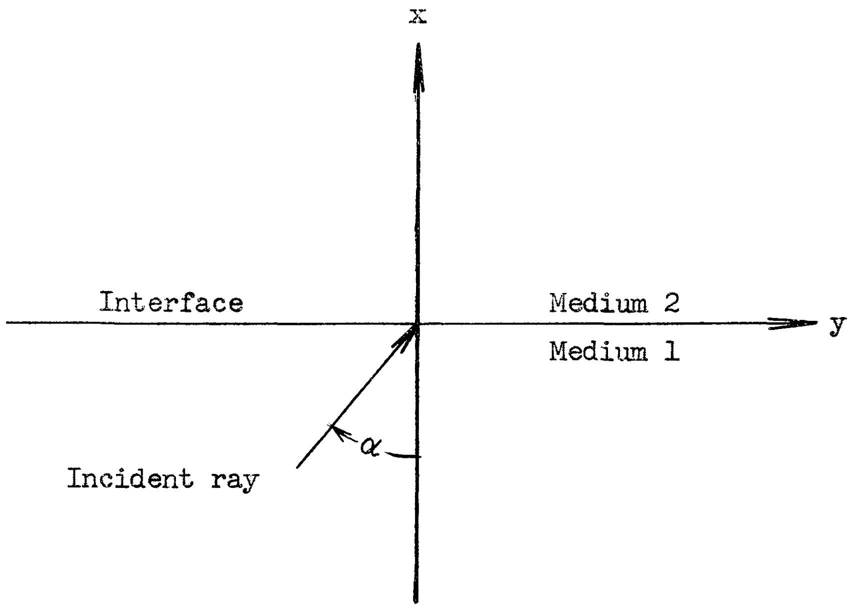

Fig. 7: Graphical representation of the problem

DISPLACEMENT FUNCTION

Let us consider fig. 7, in which the interface is represented by the plane yz, with xy being the plane of incidence. Let the positive direction of the x-axis be toward the rear, that of y to the right. The particle displacement is taken to represent the plane wave. If we denote it by ϕ, we can write

$$\phi = \phi(x,y,t)$$

If we assume that each particle executes a harmonic vibration (*), the displacement may be expressed as the real part of

(*) The assumption of a harmonic vibration does not pose any restriction. In fact, any periodic motion can be expanded into Fourier series, which can be treated as independent harmonic components.

$$\phi = K\, e^{i\, p\, f(x,y,t)} \tag{15}$$

where the proportionality factor is given by

$p = 2\pi/T$ (where T is period)

and K is displacement amplitude.

The problem now is to find f(x,y,t) for each of the five waves. After careful examination of the geometrical relations, the displacement functions (Macelwane, 1936, p. 153-154) result as

$$\phi_A = A\, e^{i\, p\, (t - \frac{y \sin\alpha + x \cos\alpha}{c_l})} \tag{16a}$$

$$\phi_C = C\, e^{i\, p\, (t - \frac{y \sin\alpha - x \cos\alpha}{c_l})} \tag{16b}$$

$$\phi_D = D\, e^{i\, p\, (t - \frac{y \sin\beta - x \cos\beta}{c_t})} \tag{16c}$$

$$\phi_E = E\, e^{i\, p\, (t - \frac{y \sin\alpha + x \cos\alpha}{c_l})} \tag{16d}$$

$$\phi_F = F\, e^{i\, p\, (t - \frac{y \sin\beta + x \cos\beta}{c_t})} \tag{16e}$$

BOUNDARY CONDITIONS

If we suppose that the two media constitute a slipping contact across which no shear stress can be transmitted, then four boundary conditions must be met at the interface:

1). Equality of the sums of the normal displacements on the two sides of the interface

$$\Sigma u_1 = \Sigma u_2 \tag{17}$$

2). Equality of the sums of the normal stresses across the interface

$$\sum(\sigma_{xx})_1 = \sum(\sigma_{xx})_2 \tag{18}$$

3). Sum of the shear stresses in medium 1 at the interface equal to zero

$$\sum(\sigma_{xy})_1 = 0 \qquad \sum(\sigma_{zx})_1 = 0 \tag{19a,b}$$

4). Sum of the shear stresses in medium 2 at the interface equal to zero

$$\sum(\sigma_{xy})_2 = 0 \qquad \sum(\sigma_{zx})_2 = 0 \tag{20a,b}$$

BASIC FORMULAS AND EQUATIONS

The cubical dilatation (Macelwane, 1936, p. 154) is given by

$$\theta = \frac{\partial u}{\partial x} + \frac{\partial v}{\partial y} + \frac{\partial w}{\partial z} \tag{21}$$

The angles α and β are related by the condition (Macelwane, 1936, p. 151)

$$\frac{\sin\alpha}{\sin\beta} = \frac{c_1}{c_t}$$

The propagation velocities (Macelwane, 1936, p. 147) in the material are given by

$$c_1 = \sqrt{\frac{\lambda + 2\mu}{\rho}} \tag{22}$$

and

$$c_t = \sqrt{\frac{\mu}{\rho}} \tag{23}$$

(These two formulas are equivalent with the ones shown on p. 7.)

The components of the normal and shear stresses (Macelwane, 1936, p. 155) may be expressed in the form

$$\sigma_{xx} = \lambda\theta + 2\mu \frac{\partial u}{\partial x} \tag{24}$$

$$\sigma_{xy} = \mu \left(\frac{\partial v}{\partial x} + \frac{\partial u}{\partial y}\right) \tag{25}$$

$$\sigma_{zx} = \mu \left(\frac{\partial u}{\partial z} + \frac{\partial w}{\partial x}\right) \tag{26}$$

The displacement components (Macelwane, 1936, p. 159) normal to the interface are (the subscript denoting in each case the source)

$$u_A = \phi_A \cos\alpha \tag{27a}$$

$$u_C = -\phi_C \cos\alpha \tag{27b}$$

$$u_D = \phi_D \sin\beta \tag{27c}$$

$$u_E = \phi_E \cos\alpha \tag{27d}$$

$$u_F = \phi_F \sin\beta \tag{27e}$$

and the components parallel to the interface are

$$v_A = \phi_A \sin\alpha \tag{28a}$$

$$v_C = \phi_C \sin\alpha \tag{28b}$$

$$v_D = \phi_D \cos\beta \tag{28c}$$

$$v_E = \phi_E \sin\alpha \tag{28d}$$

$$v_F = -\phi_F \cos\beta \tag{28e}$$

SOLUTION

For our particular case where the plane xy is the plane of incidence, no particle motion takes place in the z direction. The two generated shear waves are polarized in the plane of incidence and the particles move in only one direction.

Therefore
$$\sigma_{zx} = 0$$

$$\frac{\partial w}{\partial z} = 0$$

and
$$\theta = \frac{\partial u}{\partial x} + \frac{\partial v}{\partial y}$$

We can now apply the four boundary conditions, obtaining the following four equations (see also the appendix for a more detailed development):

a). $$A \cos\alpha - C \cos\alpha + D \sin\beta = E \cos\alpha + F \sin\beta \tag{29}$$

b). $$A c_l \cos 2\beta + C c_l \cos 2\beta - D c_t \sin 2\beta = E c_l \cos 2\beta + F c_t \sin 2\beta \tag{30}$$

c). $$-A c_t \sin 2\alpha + C c_t \sin 2\alpha + D c_l \cos 2\beta = 0 \tag{31}$$

d). $$E c_t \sin 2\alpha - F c_l \cos 2\beta = 0 \tag{32}$$

This is a system of four equations with five unknowns. We can reduce the number of unknowns to four by using the amplitude ratios

$$\frac{C}{A}, \frac{D}{A}, \frac{E}{A}, \frac{F}{A}.$$

Solving the system by determinants we find for the amplitude ratios

$$\frac{C}{A} = \frac{\sin 2\alpha \ \sin 2\beta}{k^2 \cos^2 2\beta + \sin 2\alpha \ \sin 2\beta} \tag{33}$$

$$\frac{D}{A} = \frac{k \cos 2\beta \ \sin 2\alpha}{k^2 \cos^2 2\beta + \sin 2\alpha \ \sin 2\beta} \tag{34}$$

$$\frac{E}{A} = \frac{k^2 \cos^2 2\beta}{k^2 \cos^2 2\beta + \sin 2\alpha \ \sin 2\beta} \tag{35}$$

$$\frac{F}{A} = \frac{k \cos 2\beta \sin 2\alpha}{k^2 \cos^2 2\beta + \sin 2\alpha \sin 2\beta} \tag{36}$$

where $k = \frac{c_l}{c_t}$.

It can be easily shown that these amplitude ratios apply to the stresses as well as the displacements. In fact, for harmonic motion we can write

$$F = - \text{constant} \cdot x$$

which is equivalent to

$$|\sigma| \propto |u|$$

Therefore, eqs. 33 to 36 represent the stress amplitude ratios.

The amplitude ratios given by eqs. 33 to 36 are expressed as functions of three variables: α, β, and k. As $\beta = \text{arc sin} (\sin\alpha/k)$, the amplitude ratios are in fact functions of only two of the three variables. The elimination of one of the variables, however, is not convenient, because it would extend and complicate the equations and eventually include an irrational term.

The method used to obtain the amplitude ratios is similar to the one used by Nunley (1960, p. 31-37). However, Nunley expressed his final results in a slightly different and less simplified form. A careful examination shows that the expressions for C/A and D/A are not equivalent. It appears that Nunley made a mistake in the solution of the system of four equations, which is equivalent to the system of equations obtained in this investigation (eqs. 29 to 32).

A simple way to prove the validity of the equations is by conservation of energy: the energy of the four generated waves has to be equal to the energy of the incident wave. Blut's equation of energy (1932, p. 178)

$$1 = \frac{C^2}{A^2} + \frac{D^2 \sin 2\beta}{A^2 \sin 2\alpha} + \frac{E^2}{A^2} + \frac{F^2 \sin 2\beta}{A^2 \sin 2\alpha} \qquad (37)$$

shows that energy is conserved.

A careful examination of the amplitude-ratio equations shows the following:

a). For incidence at 0° and 90°, the two transverse waves and the reflected longitudinal wave are not generated; only the transmitted longitudinal wave is formed.

b). Both the transmitted and reflected shear waves are equal in amplitude for any angle of incidence.

c). The amplitude of the transmitted longitudinal wave is the largest, the one of the transverse waves intermediate, and the one of the reflected longitudinal wave is the smallest of the amplitudes for any angle of incidence.

Fig. 8 shows the amplitude ratios as a function of the interface angle.

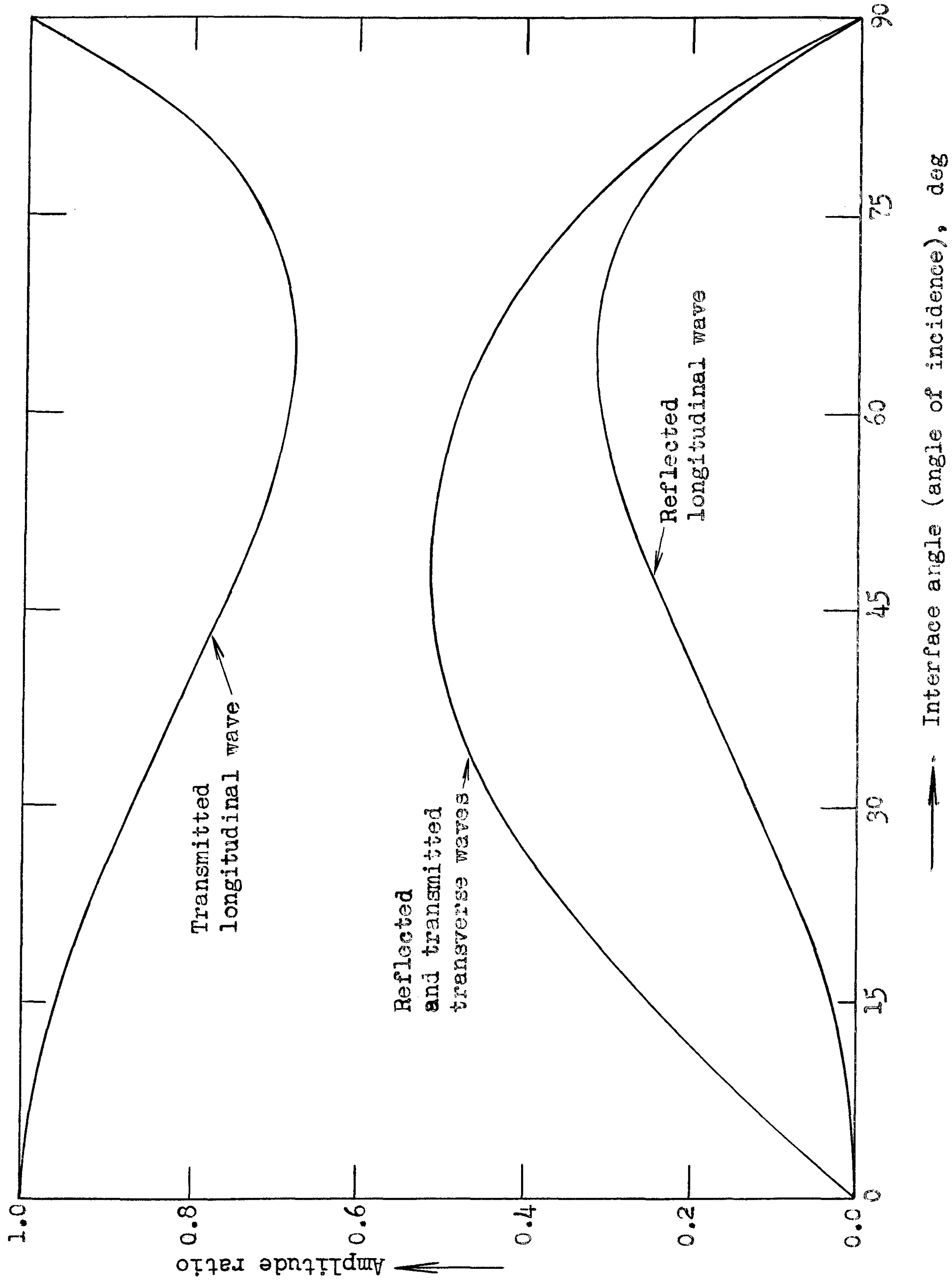

Fig. 8: Theoretical amplitude ratios vs. interface angle, for **Plexiglas**

TESTS

PURPOSE

This research consists mainly of several series of tests performed to investigate the empirical relationship for transient longitudinal stresses crossing noncohesive, oblique interfaces. More specifically, the purpose has been to determine a trigonometric expression for the relative transmitted stress as a function of the interface angle.

The experimental arrangement used in the tests is shown schematically in fig. 9. A blasting cap provides the transient stress disturbance, which is a spherically-diverging compression pulse. In the general case in which $\alpha \neq 0°, 90°$, four new disturbances will be generated at the interface. Of these four, only the transmitted longitudinal stress will be considered. This disturbance is transmitted into the pellet, and then reflected from its free surface as a tension pulse. When the reflected pulse reaches the interface between specimen and pellet, the pellet will fly off. Its velocity is proportional to the impulse trapped in it. The impulse per unit area, in turn, is given by

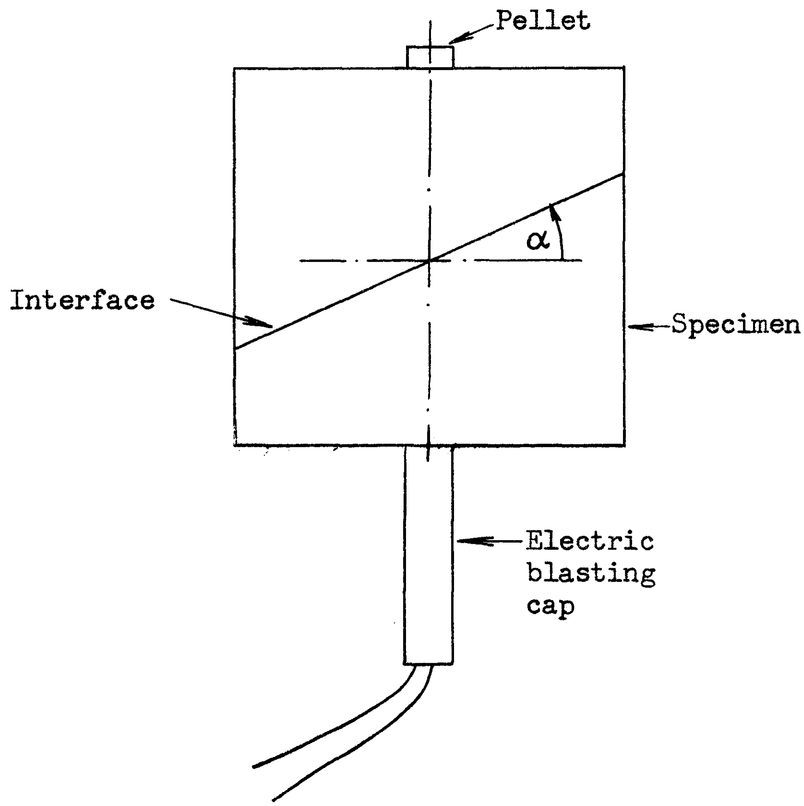

Fig. 9: Specimen design characteristics

the area under the stress-time curve corresponding to 2 times the thickness of the pellet. Or

$$\frac{I}{A} = \int_0^{2t_p/c_1} \sigma \, dt$$

where t_p is the pellet thickness.

By use of a pellet of adequate thickness, the entire impulse of the incident compression pulse can be trapped in the pellet.

It has been mentioned above that four new disturbances are generated at the interface. This follows from the assumption that conditions for a periodic motion are also applicable to this particular case of a single transient pulse. We then have at the interface:

a). an incident longitudinal disturbance,

b). a reflected longitudinal disturbance,

c). a reflected transverse disturbance,

d). a transmitted longitudinal disturbance, and

e). a transmitted transverse disturbance.

The energy of the last four pulses will be equivalent to the energy of the incident pulse.

Considering that a longitudinal disturbance travels with almost twice (8700/4400) the velocity of a transverse disturbance in Plexiglas, it can be seen that the transverse disturbance will not affect the pellet's impulse. In fact, in all but one series of tests, the interface-pellet distance was 1 in., whereas the largest pellet was only 3/16 in. thick, or $2x3/16 < 1$ in.

The average relative stress has been chosen as the magnitude to be compared. The advantage of this choice lies in the accuracy: while the average relative stress is practically measured directly, the maximum stress and particle velocity are derived magnitudes and are consequently less accurate. But if the proportionality factor across the interface is assumed independent of stress level, the graphs will also apply to stress and particle velocity amplitudes.

DESIGN VARIABLES

Interface angle (α)	0°, 15°, 30°, 45°, 60°, 75°.
Pellet thickness	1/16, 3/32, 1/8, 5/32, 3/16 in.
Distance cap-pellet	1 1/2, 2 in.
Width of specimen	1, 1 1/2, 2 in.

METHOD

The experimental setup used in this investigation has been employed successfully by Rinehart and McClain (1960) in the Mining Research Laboratory, Colorado School of Mines. The setup includes the following items: specimen, steel box, screen, camera, stroboscope and battery and wiring.

Fig. 10 shows the arrangement of these items.

The specimens and their preparation will be discussed in a following subchapter.

The steel box, in which the specimen is located, is designed to absorb the power of the explosion. It measures 15 x 19 x 28 in., and its top is covered with a heavy steel plate. A circular hole in this plate provides room for the pellet. The arrangement of the specimen in the steel box is shown in fig. 11.

The screen, with squares measuring 0.1 ft on a side, provides the distance equivalent in the picture. With the electric firing circuit open, a picture of the screen on top of the steel box was taken (f8, 1/15 sec). Then the screen was removed, and the cap was fired while the shutter was wide open (exposure time 1/15 sec). This second picture

Fig. 10: Experimental setup

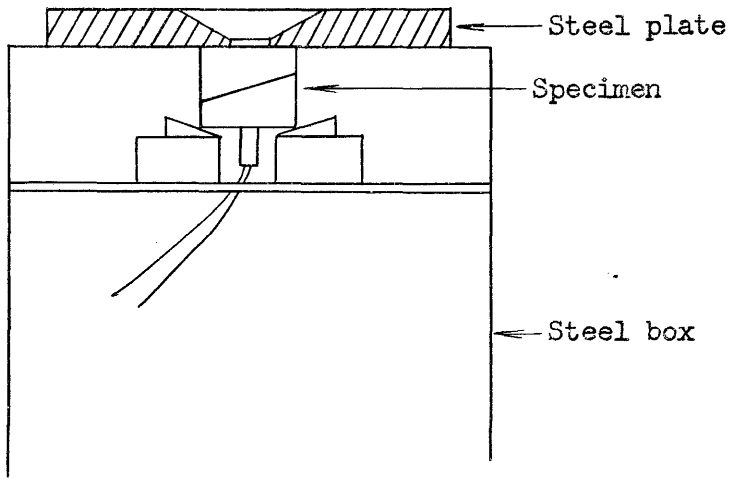

Fig. 11: Arrangement of specimen in steel box

showing the pellet in different positions is superimposed on the same film, having the screen as background.

The Polaroid camera is located at about 3 ft from the pellet's trajectory. It is equipped with Speed 3000 Polaroid film.

The stroboscope provides the necessary illumination as well as the time factor to determine the velocity of the pellet. A frequency of 6000 flashes per minute was most often used.

The wiring circuit is shown in fig. 12.

PREPARATION OF SPECIMENS

The preparation of the specimens required a considerable amount of work. Only thus was it possible to obtain homogeneous and uniform

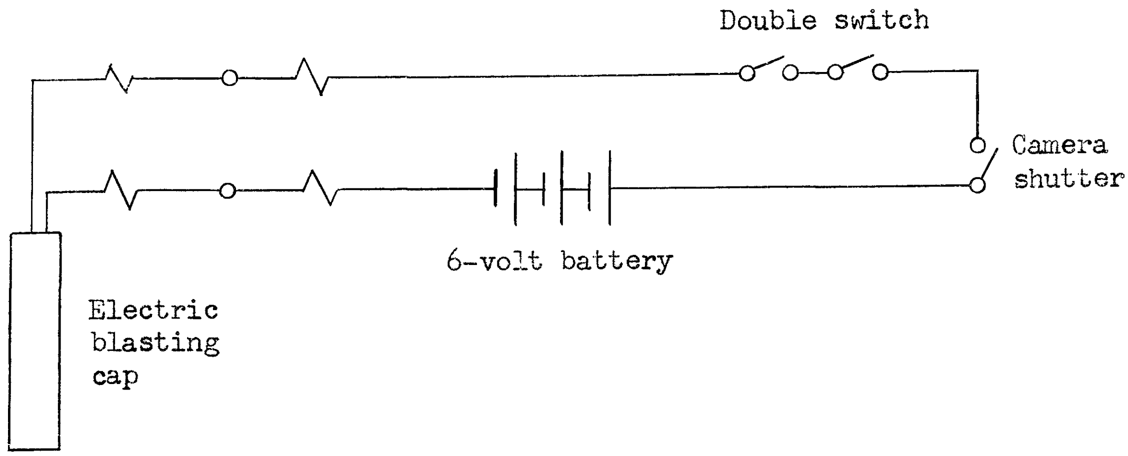

Fig. 12: Wiring circuit diagram

interfaces, and make the tests reproducible. All specimens were prepared from Plexiglas sheets, of 1-, 1 1/2-, and 2-in. nominal thickness.

A typical specimen consisted basically of three parts (see also fig. 9).

a). The electric blasting cap, which provided the transient stress pulse. Olin #6 instantaneous electric blasting caps (Plas-T-Cap) were used consistently throughout the experiments. It is assumed that the pulses developed by these caps are nearly constant and vary only within very close limits.

b). The body of the specimen -- or simply the "specimen" as used in this thesis -- consisting of two matching parts of Plexiglas, and including the interface.

c). The pellet, made out of 1/4 in. circular Plexiglas rods.

The preparation of the specimens involves the following steps:

i). drawing the specimen contour on the paper cover of the Plexiglas sheet, with enough margin for cutting and polishing;

ii). cutting out the specimens with a band saw;

iii). smoothing out the rough surfaces left by the band saw. This was done with a disc grinding-machine, using silicon carbide cloth discs;

iv). polishing finally by hand with Durite sand paper.

The two parts composing the specimen are fixed together with filament scotch tape. The blasting cap is attached in a similar way.

Different types of interface layer were tested. In most of the tests, a film of oil was placed between the two contacting surfaces of the interface. In some instances, and to provide a means of comparison, no oil or viscous grease was used. This comparison shows that the thin oil film affects the transmission coefficient very little, if at all, while at the same time the uniformity of results is greatly improved.

With a similar purpose, a film of oil was placed between specimen and pellet.

MEASUREMENTS AND CALCULATIONS

It has been explained before that the pellet flies off with a certain impulse trapped in it. From this velocity, other magnitudes can be calculated by simple mathematical relations. The velocities obtained in the experiments range from 5 to 27 m/sec.

VELOCITY MEASUREMENTS

As most of the data were derived from the velocity of the pellet, it was essential to obtain reliable and accurate measurements. Fig. 13 shows a typical double-exposure Polaroid picture, which includes all the data required to calculate the velocity.

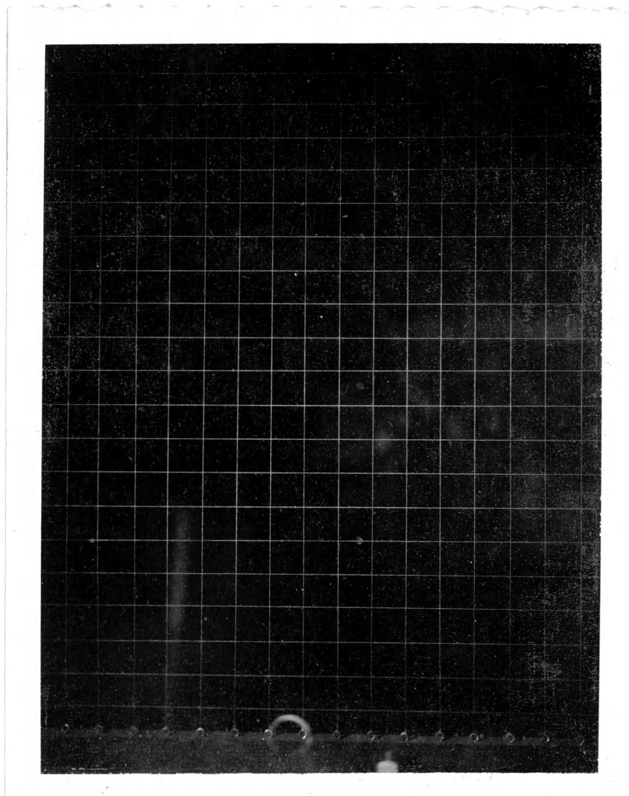

Fig. 13: Typical picture of Polaroid camera, f = 6000

The actual distance between two pellet images is given by

$$D_{act} = D_{meas} \times 30.48/CF$$

where D_{act} is actual distance

D_{meas} is distance measured on the picture

CF is conversion factor, distance of 1 ft measured on the picture

30.48 = equivalent of 1 ft in cm.

The time is given by the frequency f:

$$t = 60/f$$

and the pellet velocity is then

$$v = D_{act}/t$$

CALCULATIONS

The impulse per unit area is calculated by

$$I/A = \rho\, t_p\, v \tag{38}$$

which for a certain pellet thickness is equivalent to a constant multiplied by the velocity. This equation results from Newton's second law

$$I = m\, v$$

By replacing m by $m = \rho\, A\, t_p$

we obtain eq. 38.

The total impulse per unit area of the disturbance can be defined as that impulse corresponding to a point on the horizontal part of the curve I/A vs. time.

The stress σ is given by the slope of the curve $I/A = f(\text{time})$. In fact, we can write

$$I/A = \int F\, dt/A = \int \sigma\, dt \tag{39}$$

Taking the derivative on both sides, we finally obtain

$$\frac{d}{dt}\left(\frac{I}{A}\right) = \sigma \tag{40}$$

The particle velocity is related to the stress by the equation

$$\sigma = \rho\, c\, v$$

which gives

$$v = \frac{\sigma}{\rho\, c}$$

The average relative stress is represented by a quotient

$$\frac{\text{Average stress}\ \alpha^\circ}{\text{Average stress}\ _{\alpha=0^\circ}} \tag{41}$$

The average stress itself is given by the area under the stress-time curve divided by the duration of the pulse.

From fig. 14:

$$\text{Average stress} = \frac{1}{T}\int_0^T \sigma\, dt$$

But

$$\int_0^T \sigma\, dt = I_{tot}/A$$

and then

$$\text{Average stress} = I_{tot}/A\ T \tag{42}$$

(This calculation neglects the small area under the stress-time curve for $t>T$. The curve actually does not reach the abscissa for $t=T$, but tends to zero very slowly.)

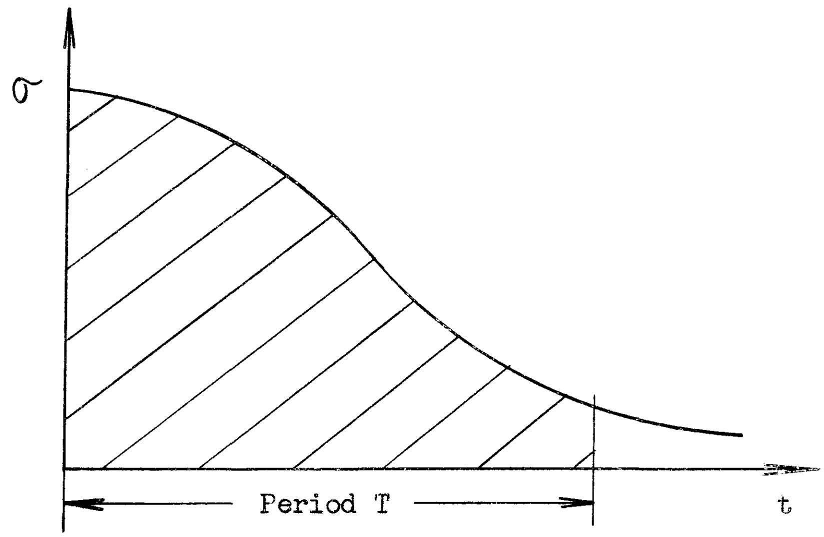

Fig. 14: Representation of average stress

SHAPE OF TRANSIENT PULSE

A primary test was performed with the purpose of describing the characteristics of the transient pulse. The experimental setup, shown in fig. 15, was essentially the same as the one used in the general group of tests, except that there was no interface.

The thickness of pellets used ranged from 1/64 to 5/8 in. The specimens had a section of 2 x 2 in. -- as shown in the figure -- 2 1/2 x 2 1/2 in., and 3 x 3 in. The purpose of this increase in section was to avoid interference of pulses reflected from the sides of the specimen. In fact, for certain "critical" pellet thicknesses (and a given specimen section) the reflected pulses would interfere and contribute

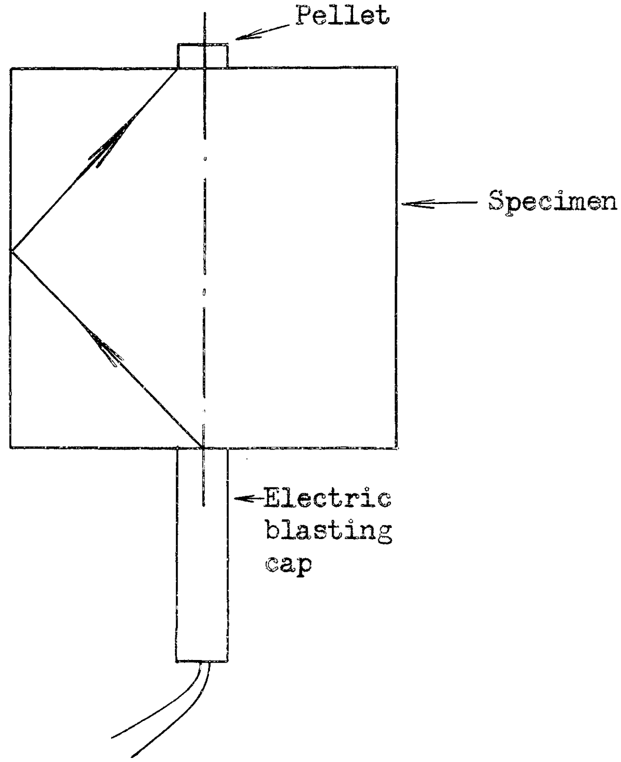

Fig. 15: Specimen used in pulse-shape test

to the impulse of the pellet. A substantial distortion of the results would be the consequence.

From Rinehart and Pearson (1954, p. 38) it is seen that a compression pulse will be reflected as a tension pulse: with $\nu = 0.4$, and $\alpha = 40°$, the coefficient of reflection results as R = -0.8. In other words, the reflected tension pulse is relatively strong, and should not be allowed to reach the pellet.

The following table shows a list of critical pellet thicknesses for different specimen sections. The critical pellet thickness can be defined as the largest pellet for which <u>no</u> interference of reflected waves will take place. The figures were obtained by a graphical method:

Specimen length	Section	Critical thickness
2	1 x 2 in.	$\approx 3/32$ in.
2	1 1/2 x 2	$\approx 7/32$
2	2 x 2	$\approx 3/8$
2	2 1/2 x 2 1/2	$> 17/32$
2	3 x 3	$> 3/4$

The results of the pulse-shape test are shown in figs. 16 and 17. In drawing these two graphs, it is assumed that the pulse is a sharp-fronted disturbance which decreases to zero stress in a uniform fashion. To meet these two assumptions, the curve in fig. 16 has been drawn accordingly without strictly following the experimental points. At the same time, the relatively high drag effect upon very thin pellets may well explain the fact that the corresponding experimental points lie below the actual curve. Fig. 17 is a stress vs. time graph, which represents the shape of the pulse in Plexiglas at a distance of 2 in. from the electric blasting cap.

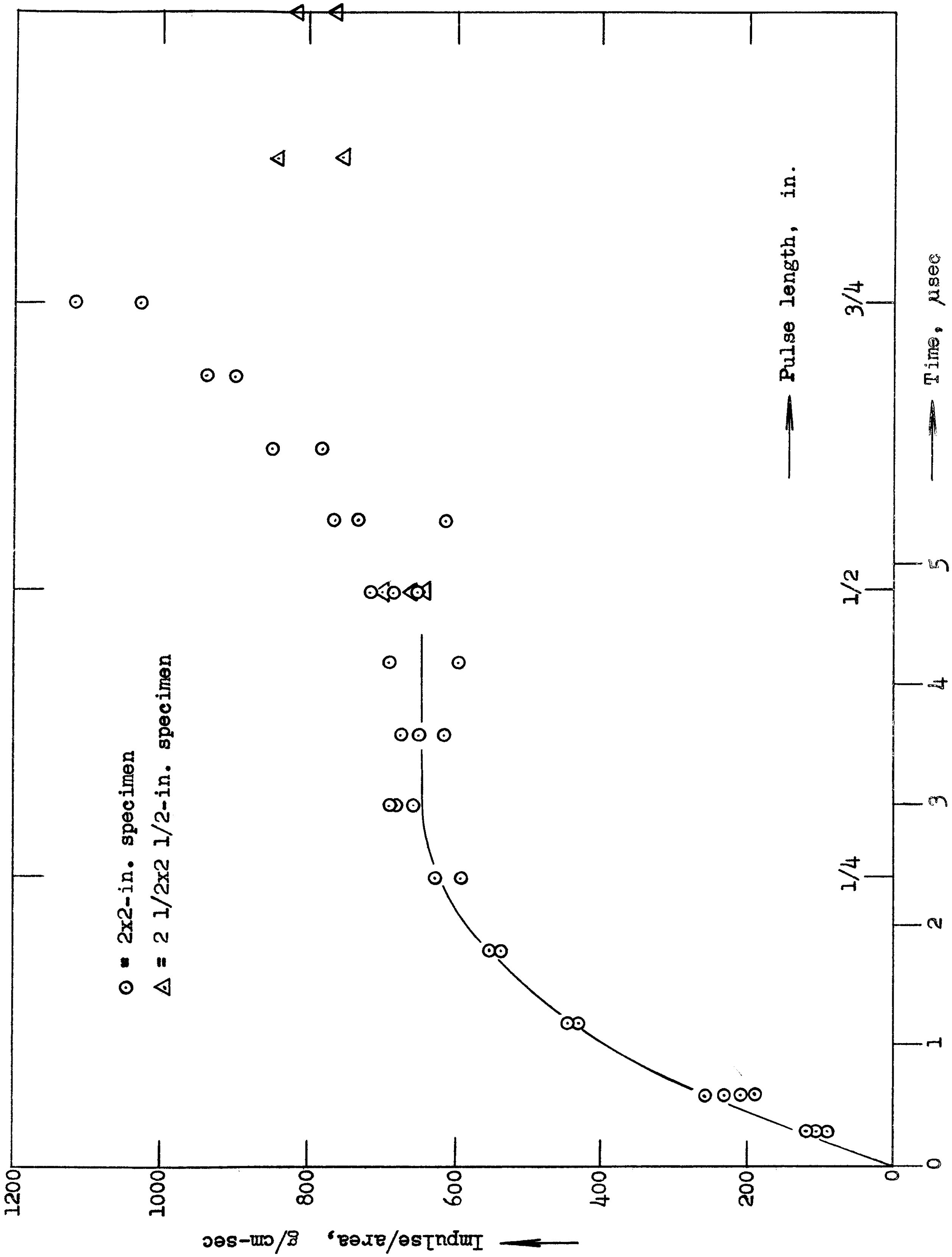

Fig. 16: Impulse per unit area vs. pulse length and time, transient pulse

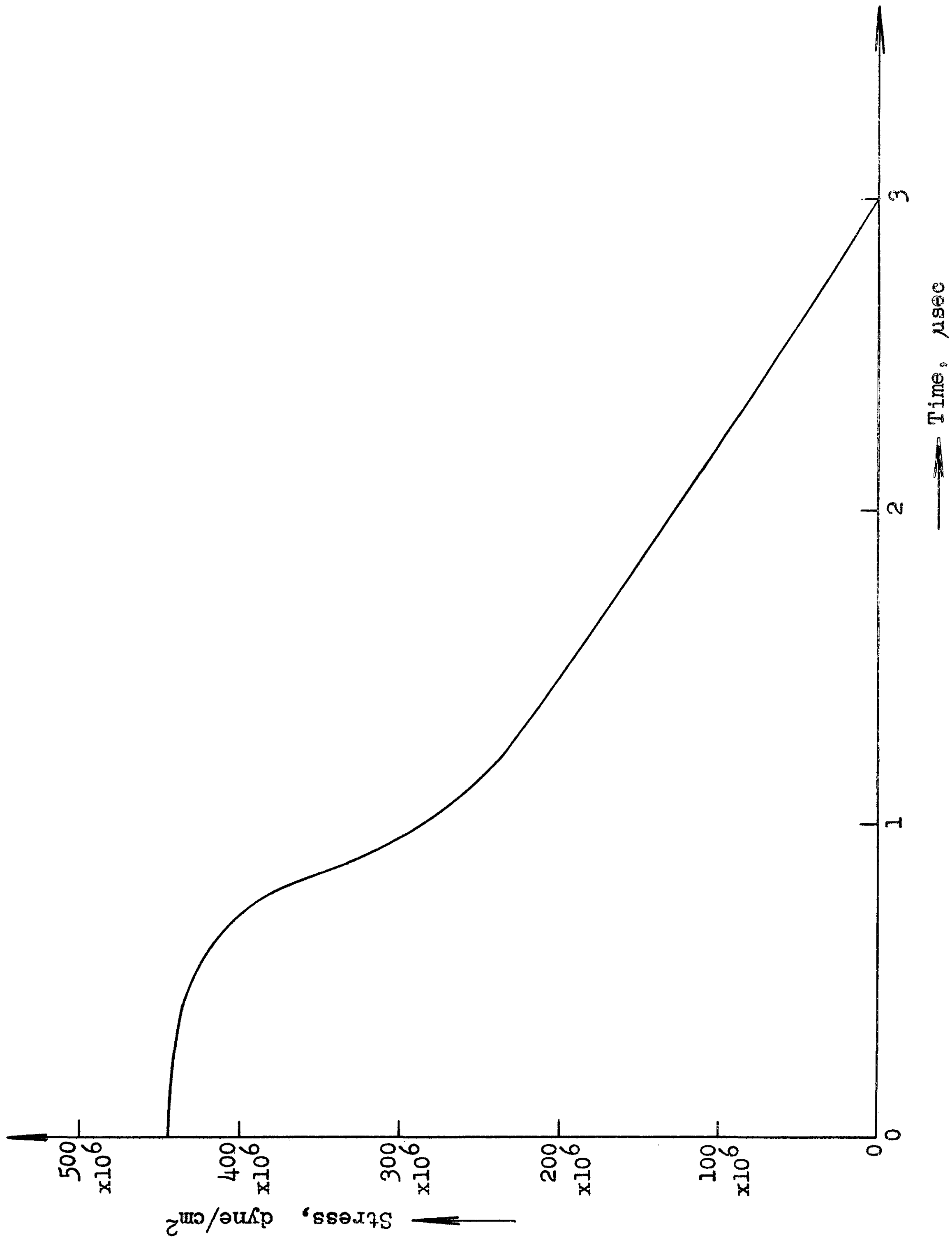

Fig. 17: Stress vs. time, transient pulse

DATA AND RESULTS

In this chapter, the data and results from the tests are shown in the form of graphs. The bulk of the data is shown in tabular form in the appendix.

The interface series comprise nearly 500 tests. This number includes six different types of specimen, with regard to specimen shape and interface layer. The four specimen shapes are shown in figs. 18, 21, 24, and 27; the types of interface layer are: oil film, grease film, and no film (air).

For each of the specimens two variables were involved:

Interface angle (α) 0°, 15°, 30°, 45°, 60°, 75°.

Pellet thickness 1/16, 3/32, 1/8, 5/32, 3/16 in.

(In series F and J only pellets of 1/16, 3/32 and 1/8 in. were used.)

For each combination of interface angle and pellet thickness three tests were performed. This was done with the purpose of reducing the effect of misfires or defective tests.

Each of the six specimen types will be considered separately in this chapter. The figure showing the specimen shape and characteristics will be followed each time by two graphs: an impulse per unit area vs. time graph, and an average relative stress vs. interface angle graph.

In this last graph, the theoretical curve (eq. 35, p. 25) will be shown for comparison.

SPECIMEN A

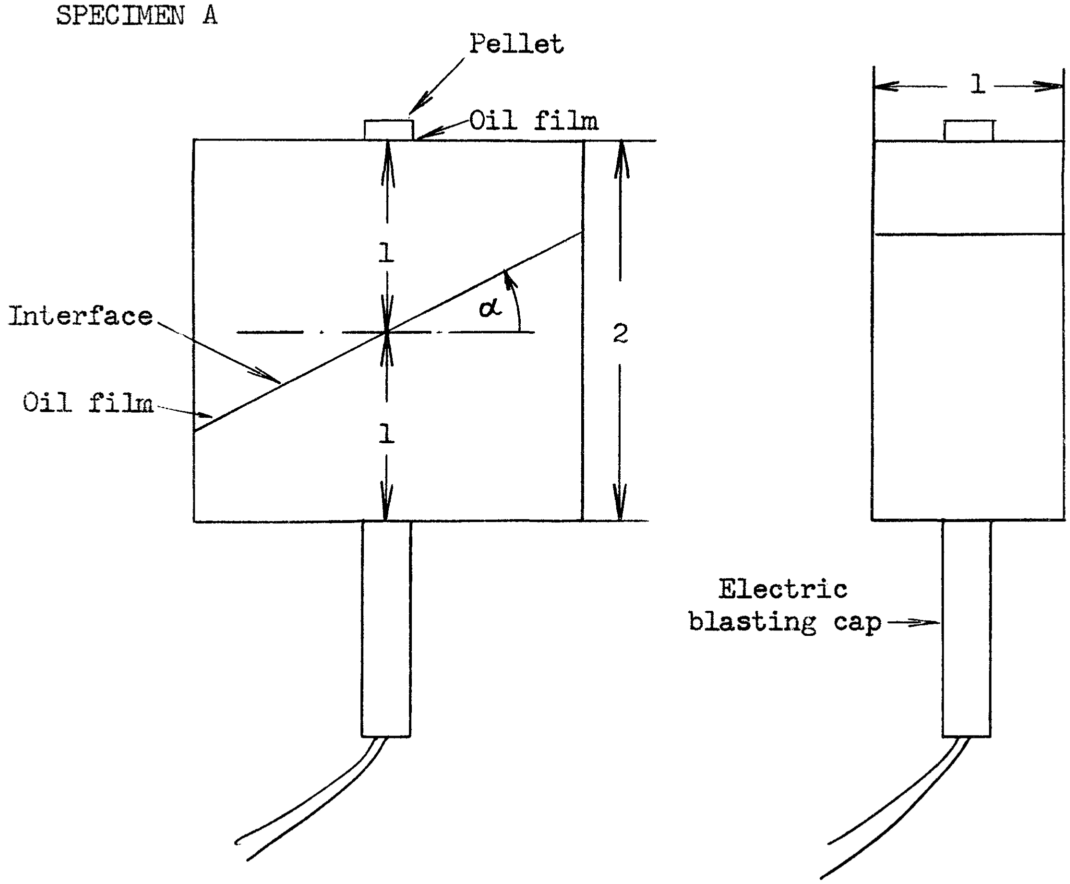

Fig. 18: Design characteristics of specimen A

The specimen-A test basically represents the transmission of a pulse across a plane oblique interface. At the same time, it approaches the transmission of a plane wave, if the rays reaching the pellet are considered parallel. This test was the first performed in this investigation. It was found, among other things, that the specimen size (and particularly the width, which was the smallest dimension) had an effect upon the impulse of the pellet. It appeared as if pulses being reflected from the sides of the specimen had a close relationship with this effect, which disappeared for specimens with greater width. For this reason, the following specimen types show either a decrease in the cap-pellet distance or an increase in the section.

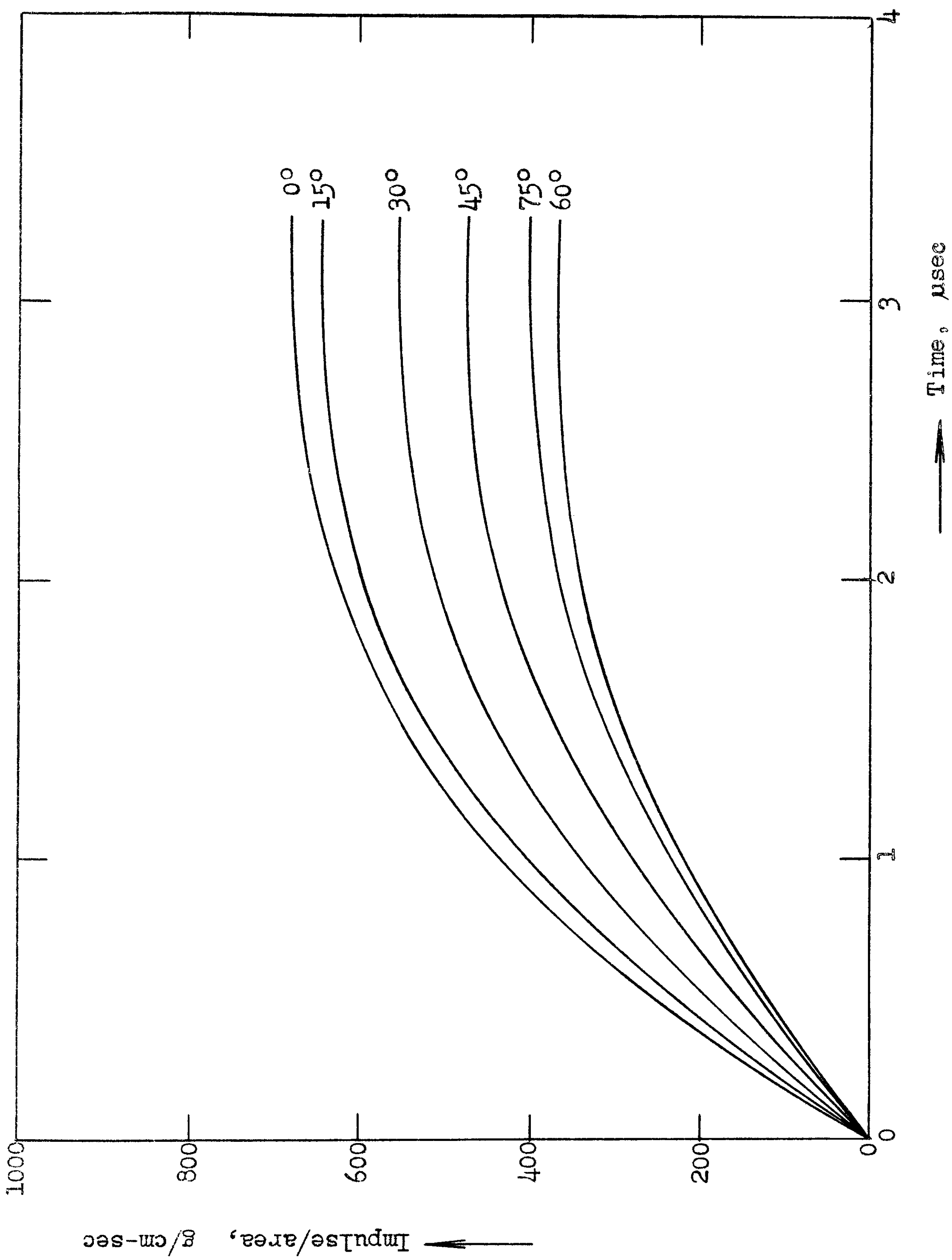

Fig. 19: Impulse per unit area vs. time, specimen A

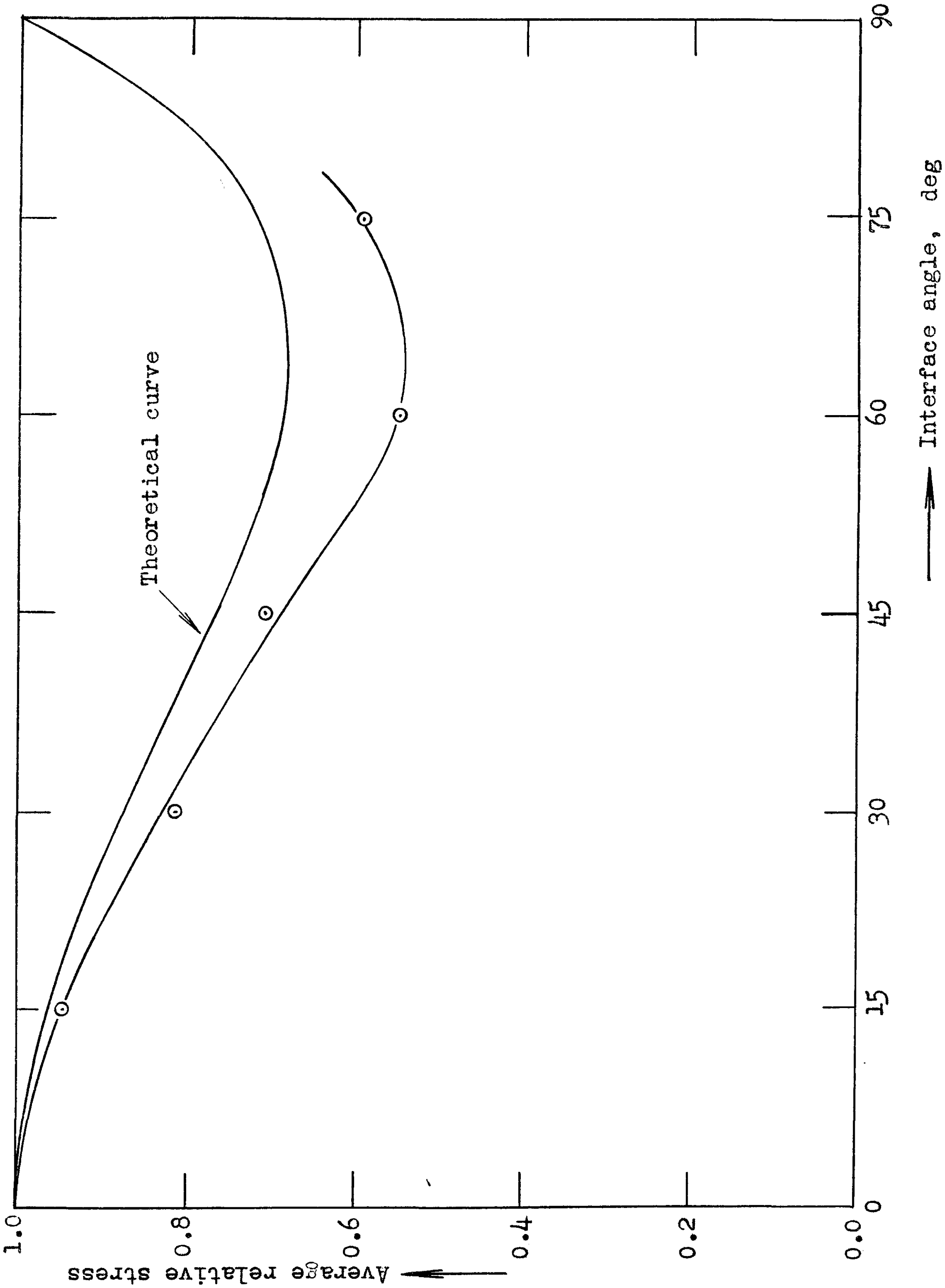

Fig. 20: Average relative stress vs. interface angle, specimen A

SPECIMEN B

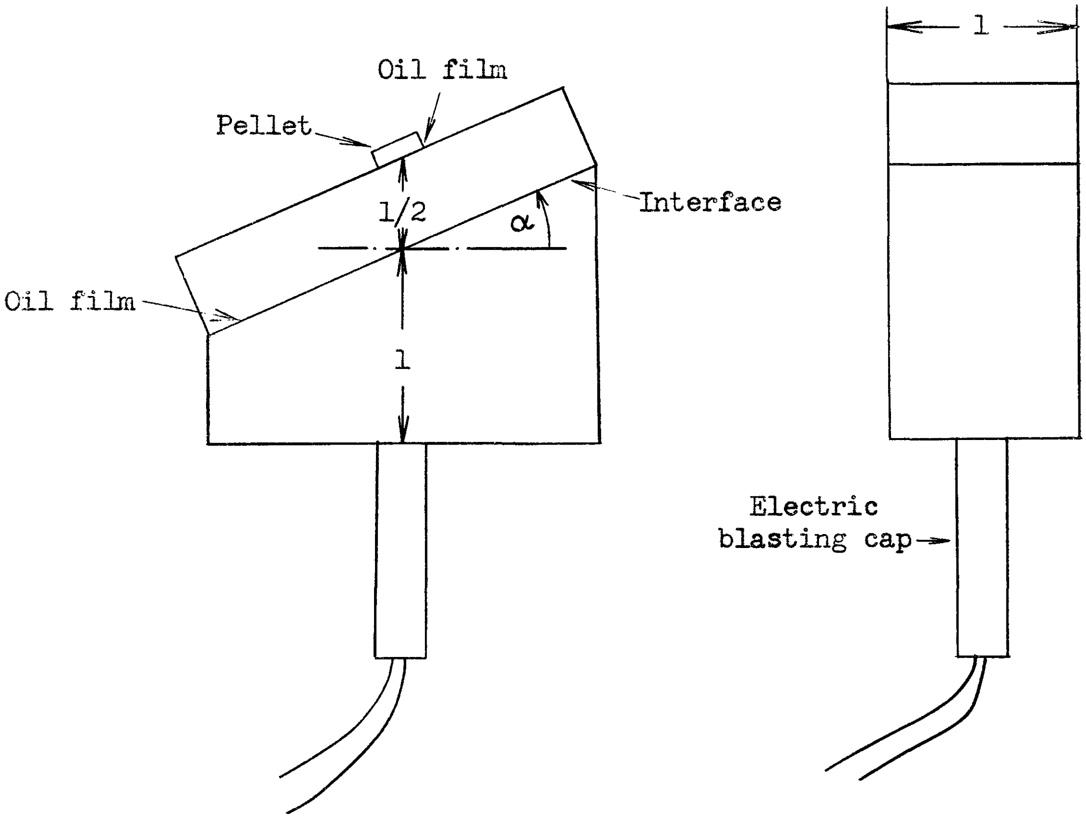

Fig. 21: Design characteristics of specimen B

Specimen B was designed with the idea of duplicating the effect of an oblique interface. In fact, the specimen contains two interfaces, both having the same angle of obliquity: one formed by the two parts of the specimen and another one between specimen and pellet. As a consequence, the transmission factor (average relative stress) would appear as the second power of the transmission factor for a single interface. Therefore, the graphical representation of $\sqrt{\text{average relative stress}}$ vs. interface angle is included in fig. 23, which shows the results of this particular test.

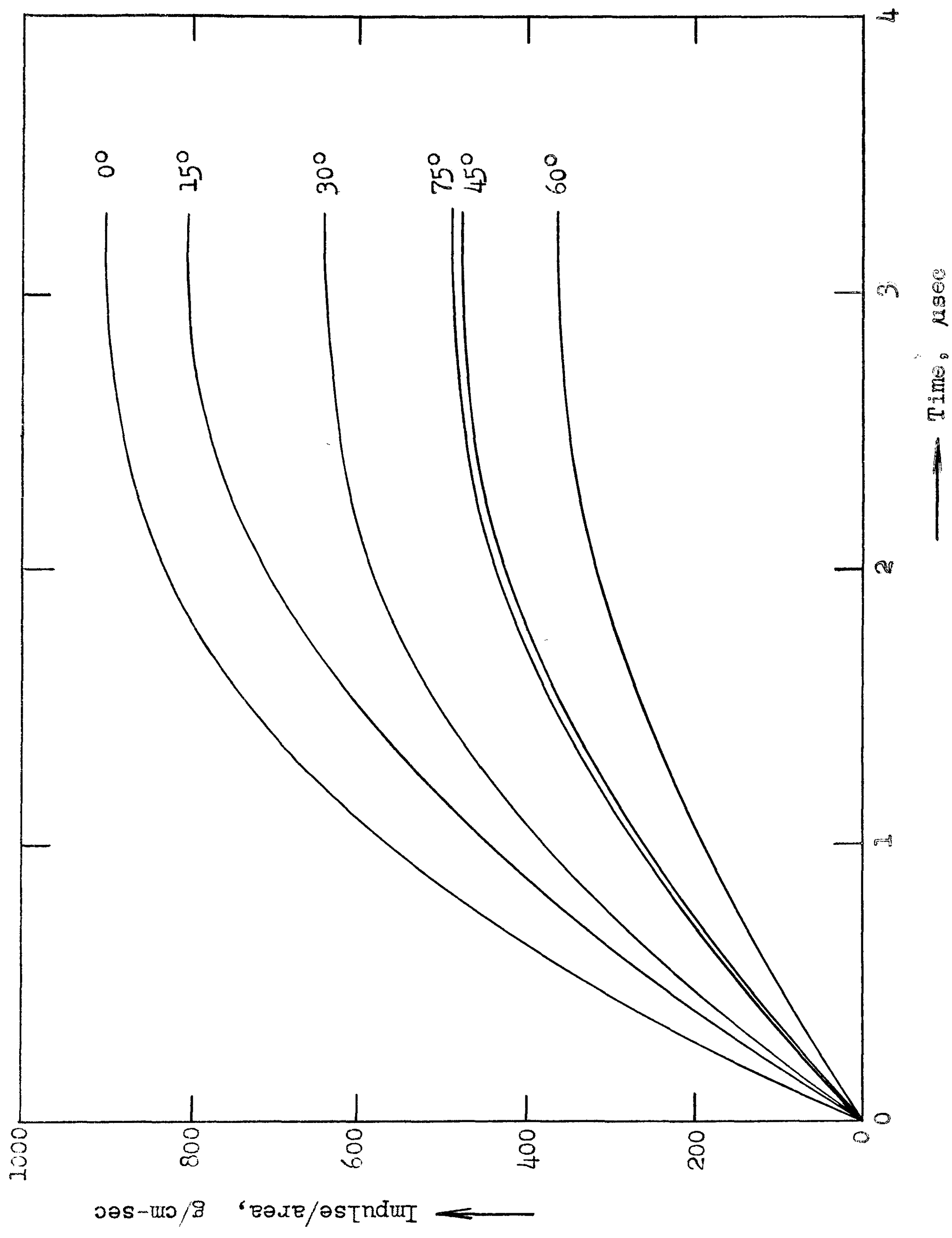

Fig. 22: Impulse per unit area vs. time, specimen B

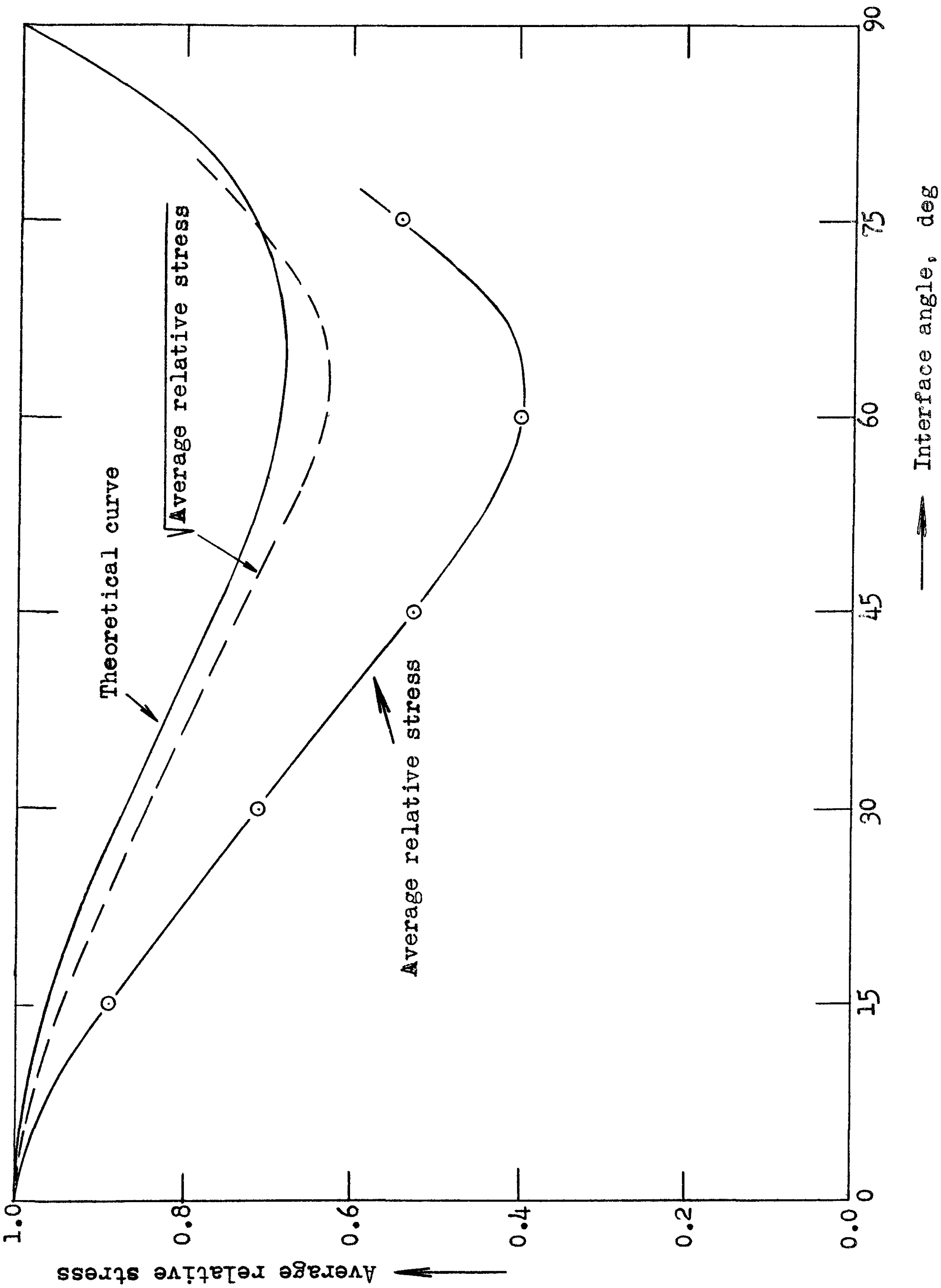

Fig. 23: Average relative stress vs. interface angle, specimen B

SPECIMEN C

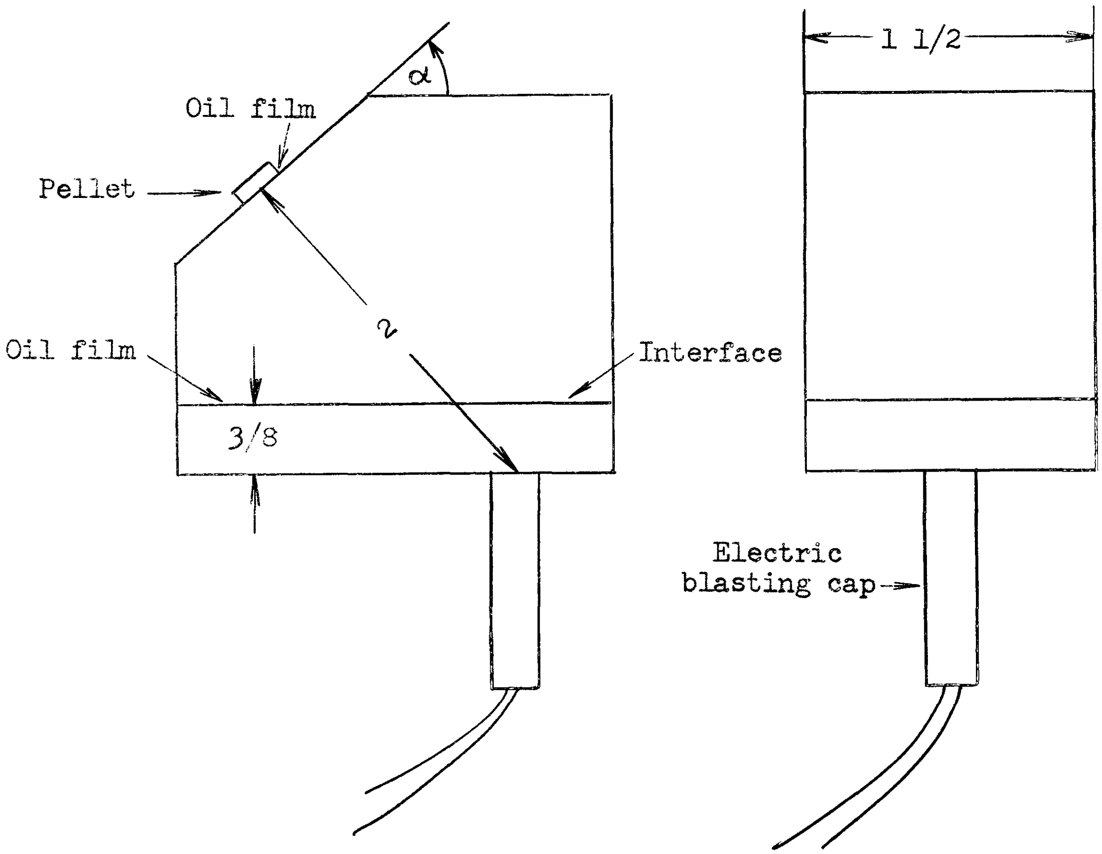

Fig. 24: Design characteristics of specimen C

The specimen-C test was aimed at determining the distribution of stresses along a circle for a spherically-diverging disturbance crossing a plane interface. Under these circumstances, the relative position of the interface changed with the angle of obliquity. It appeared, however, that this change did not affect the impulse being transmitted into the pellet.

A successful development in this test implied that the pulse generated by the blasting cap was perfectly spherical, with an even distribution of stresses along concentric spheres. This was not quite true: the stress pulses appeared to weaken with increasing angle of obliquity. Rinehart and McClain (1960, p. 1813) found that the maximum decrease was at 90° obliquity and equal to about 18 percent of the stress pulse entering normally into the specimen.

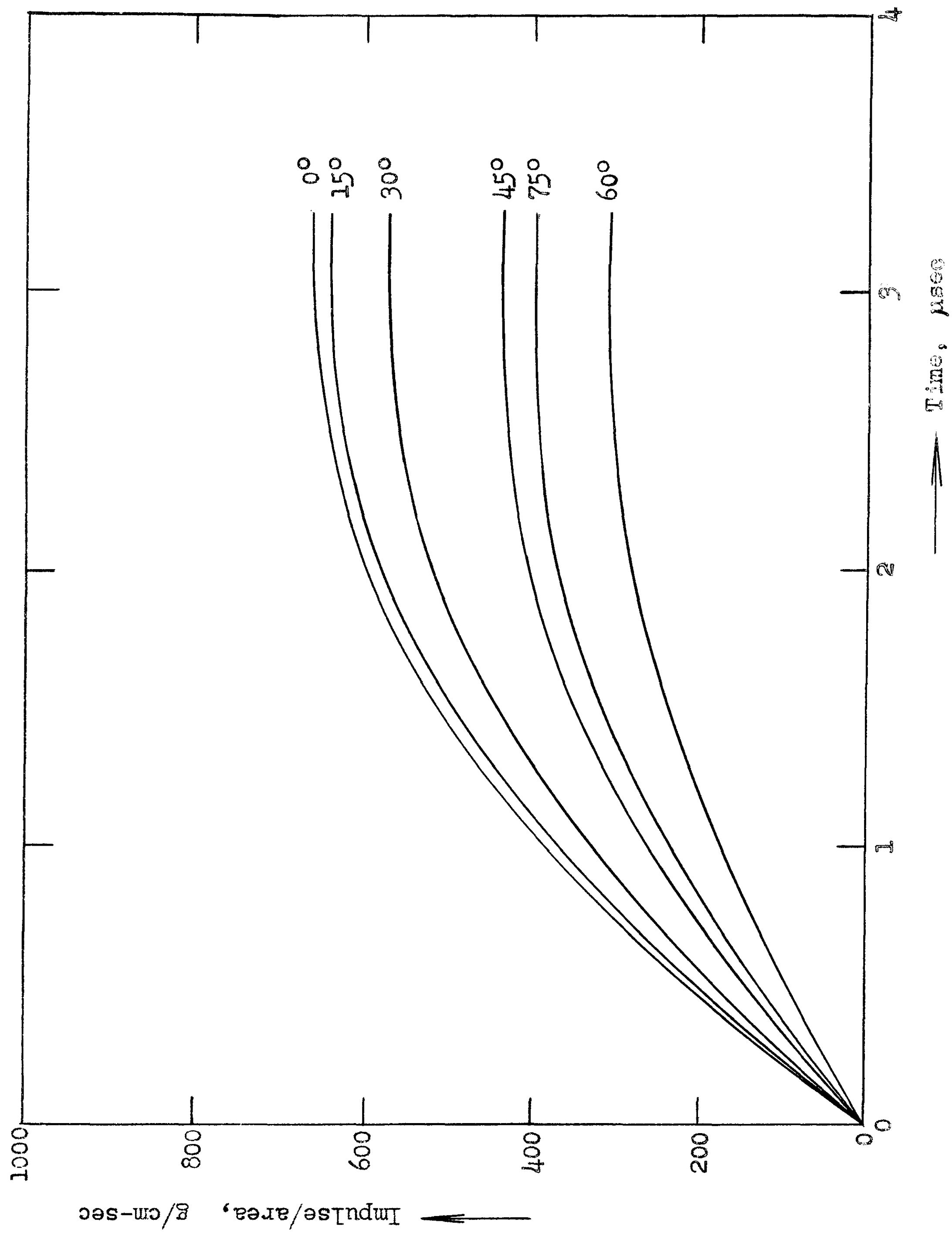

Fig. 25: Impulse per unit area vs. time, specimen 6

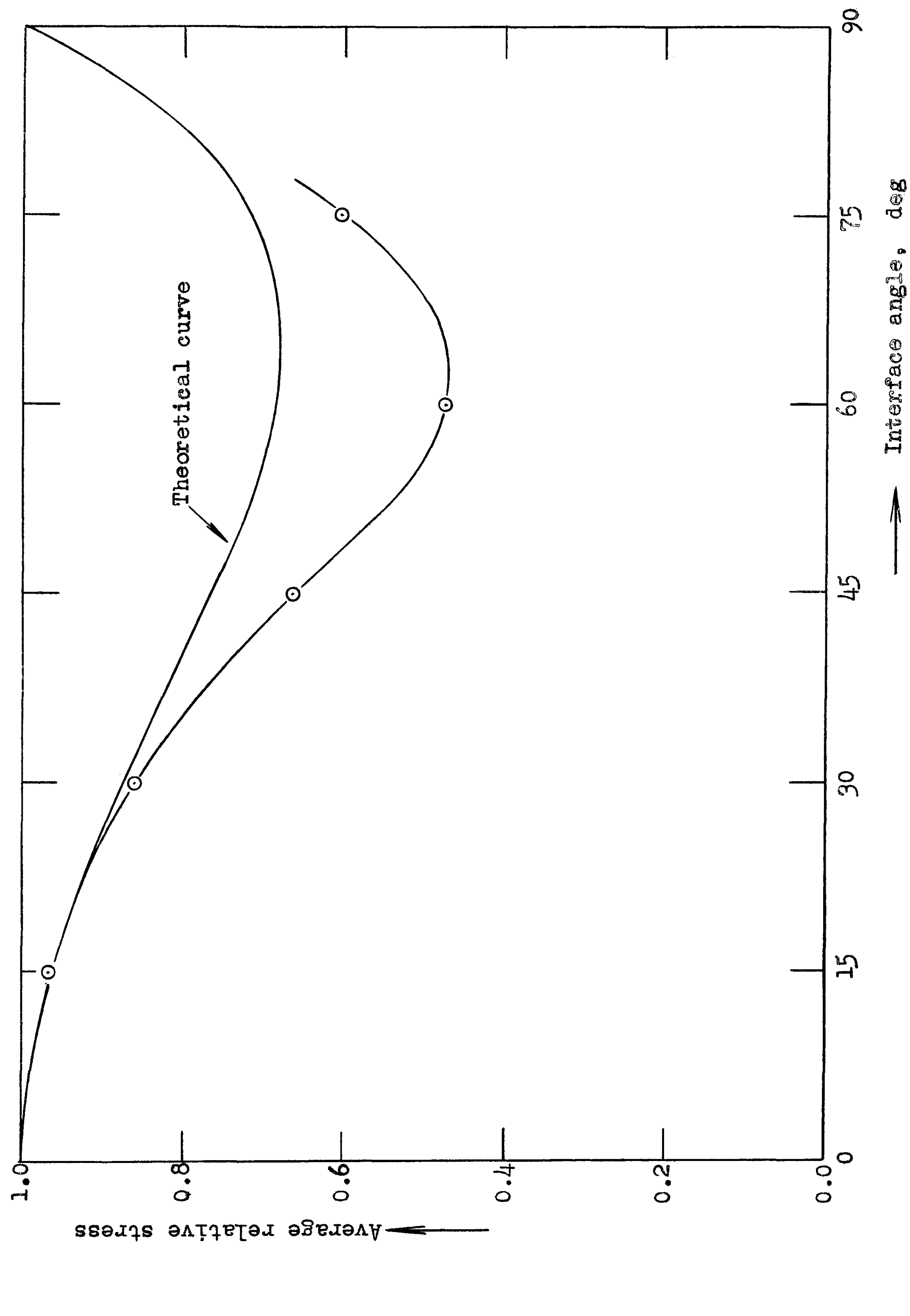

Fig. 26: Average relative stress vs. interface angle, specimen C

SPECIMEN E

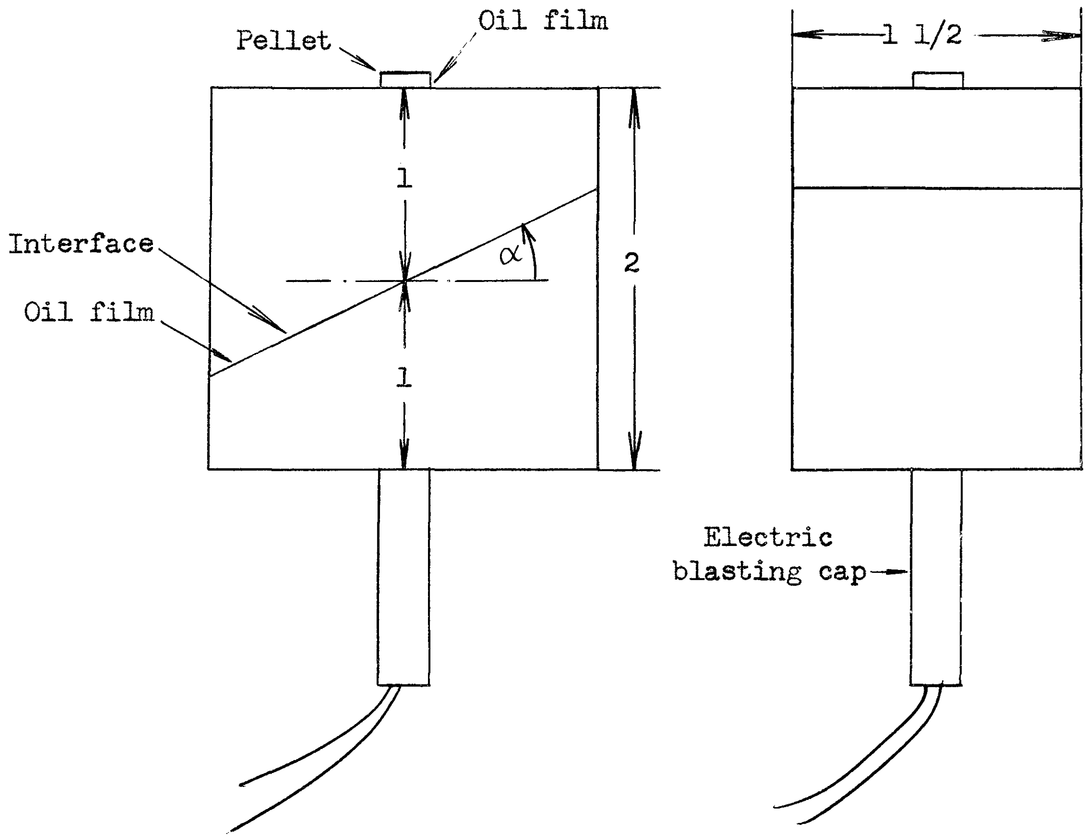

Fig. 27: Design characteristics of specimen E

Specimen E was similar in all its features to the specimen A, except for its width, which was 1 1/2 in. rather than 1 in. The unusual increase of impulse of the larger pellets (3/16 in.) observed in tests with A-type specimens disappeared with the increase in width. This simplified and made more accurate the determination of the total impulse per unit area of the disturbance.

Up to this point, all specimens had a thin oil film at the interface.

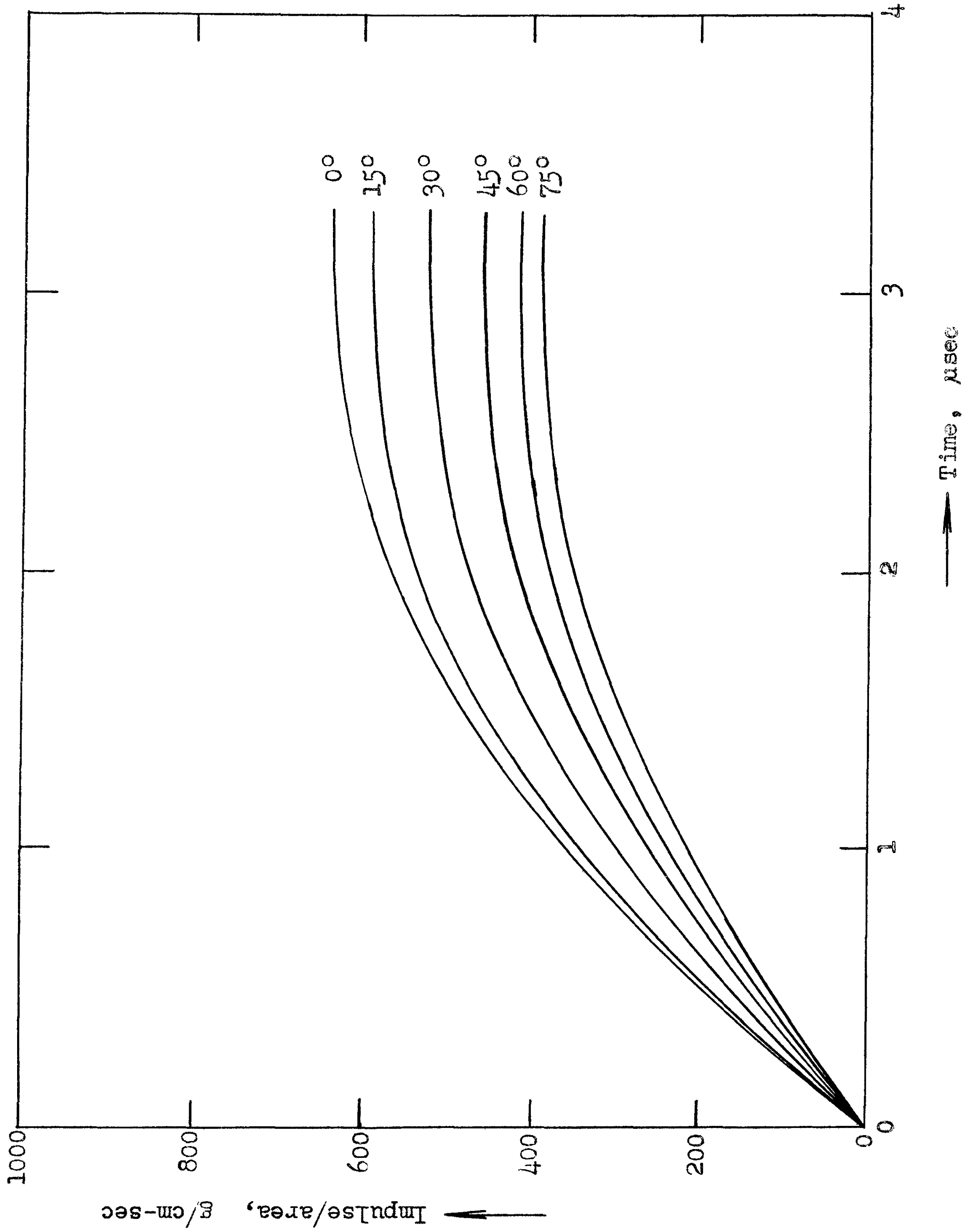

Fig. 28: Impulse per unit area vs. time, specimen E

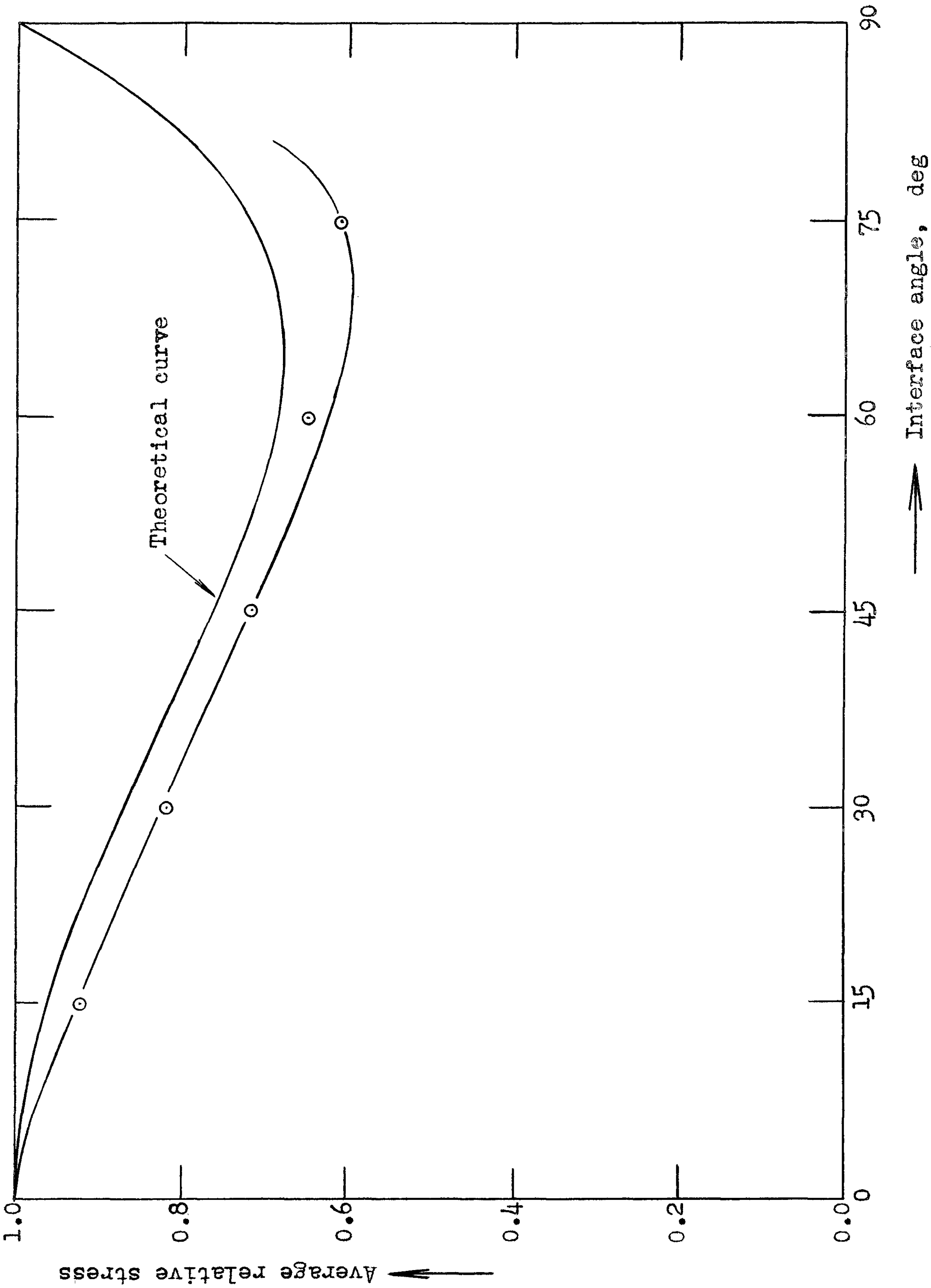

Fig. 29: Average relative stress vs. interface angle, specimen E

SPECIMEN F

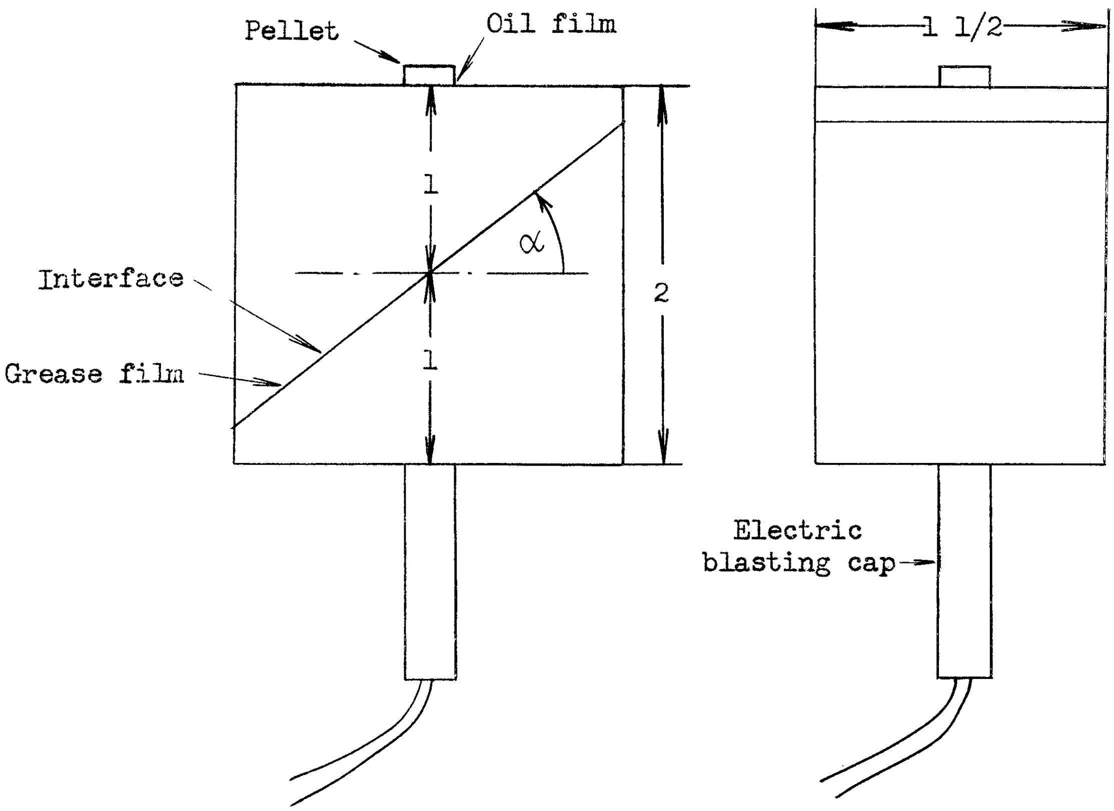

Fig. 30: Design characteristics of specimen F

The particular feature of this specimen was the grease film at the interface. The test was designed to provide a comparison for the tests with an oil film. It was observed that although more uniform results were obtained with the grease-film tests, the final results were the same. In other words, the film at the interface did not seem to have a decisive influence upon the pulse transmission.

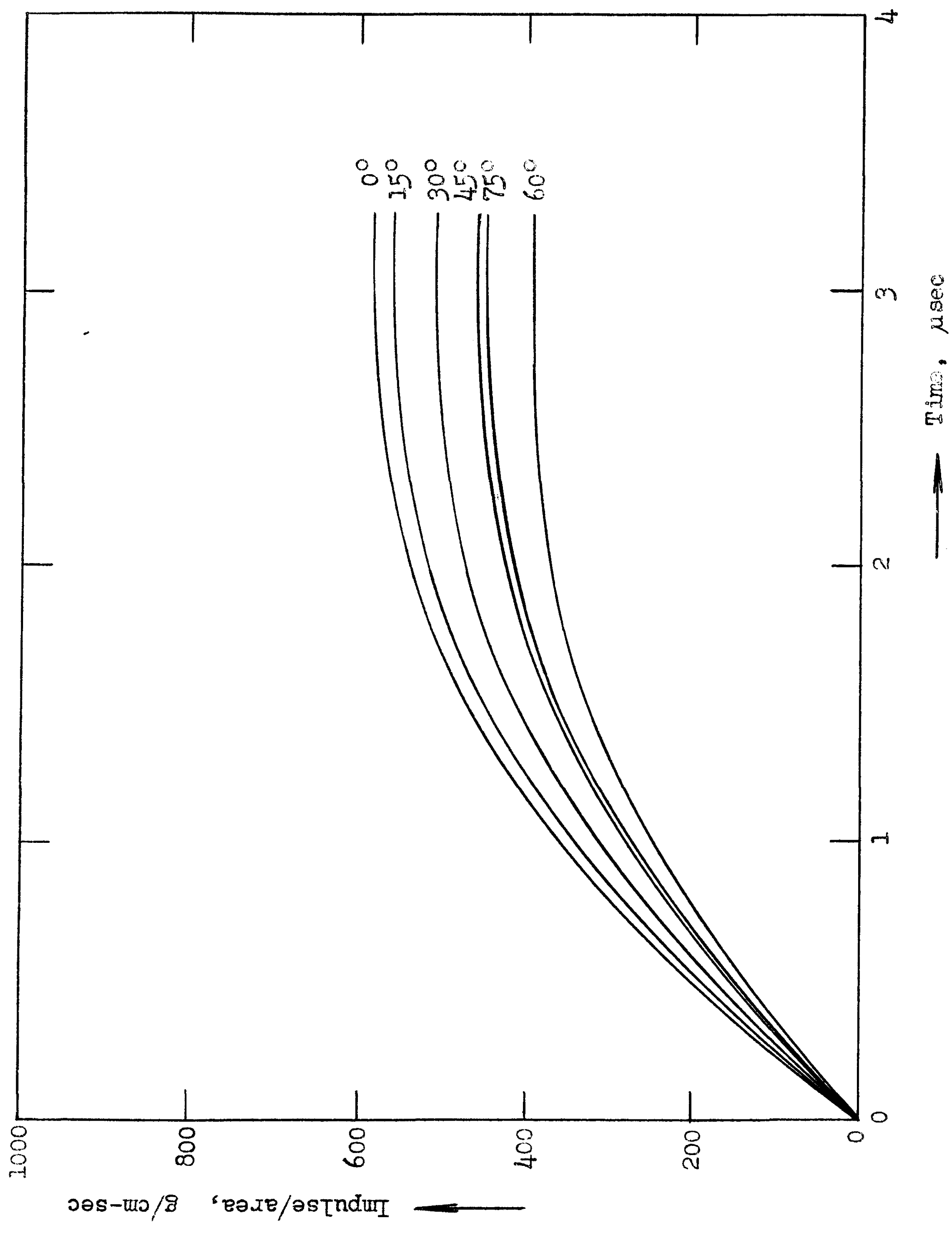

Fig. 31: Impulse per unit area vs. time, specimen F

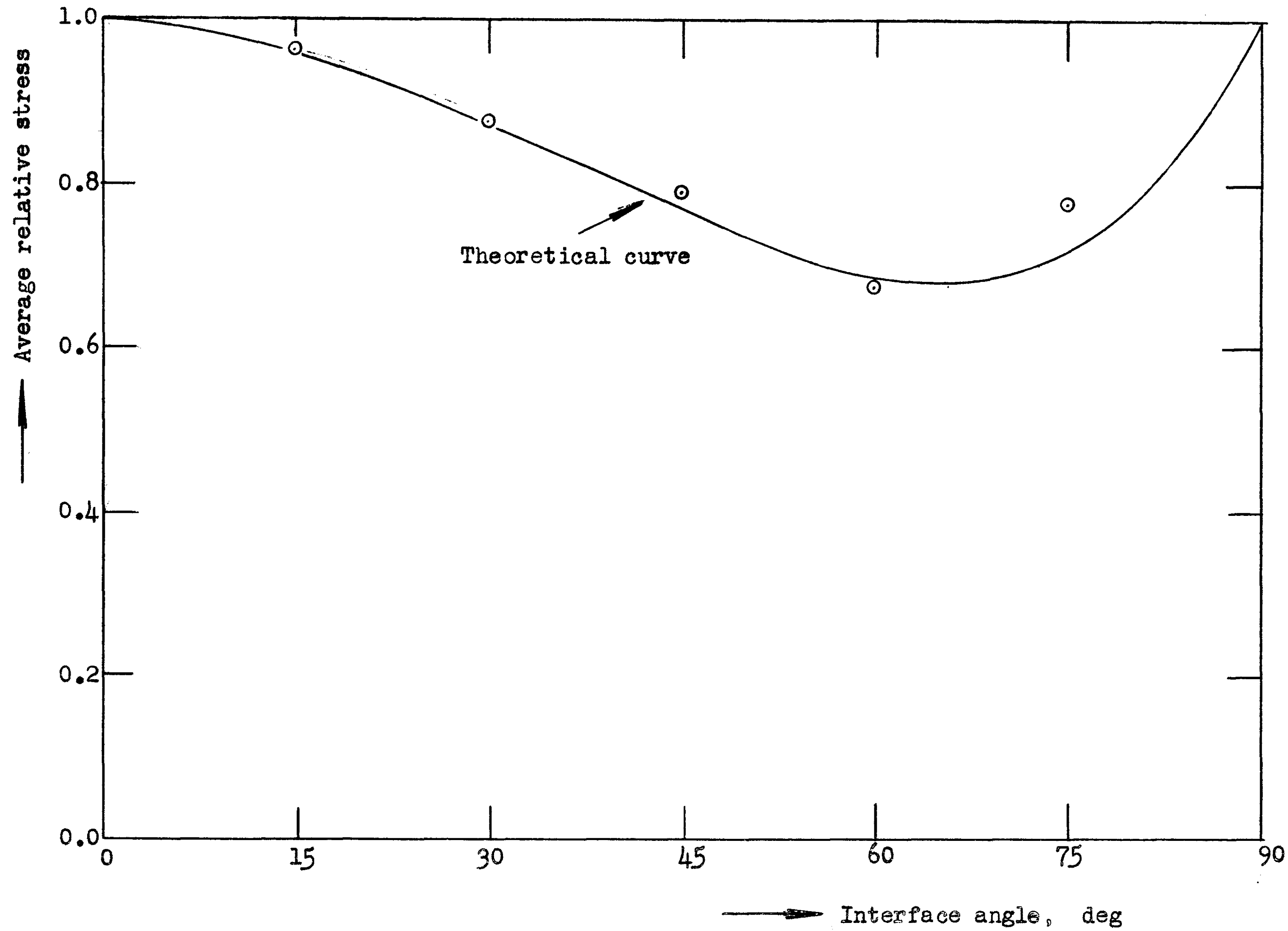

Fig. 32: **Average relative stress vs. interface angle, specimen F**

SPECIMEN J

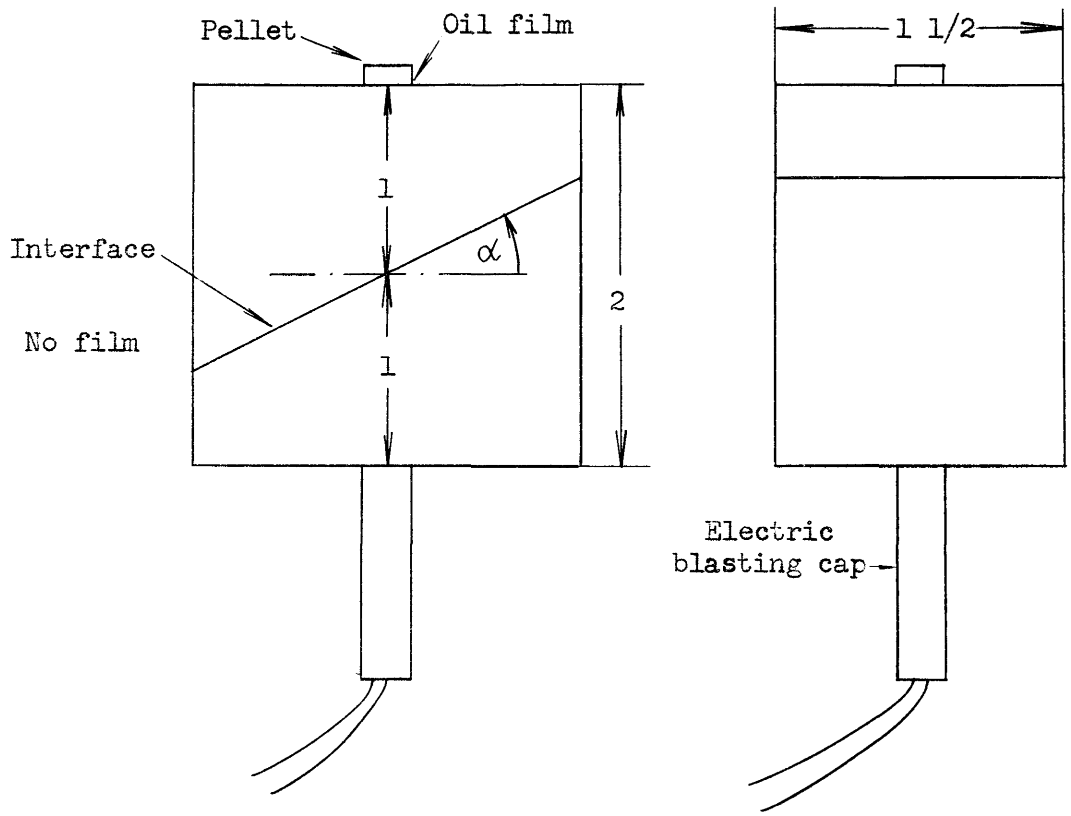

Fig. 33: Design characteristics of specimen J

In this particular case there was neither an oil film nor a grease film at the interface. The measurements obtained were somewhat nonuniform, but the results followed the same trend of the other tests. It seemed that the scattering of the plotted data was caused by the rather occasional contact of the two surfaces forming the interface. It was not possible to avoid this effect even by a careful polishing of the two mentioned surfaces.

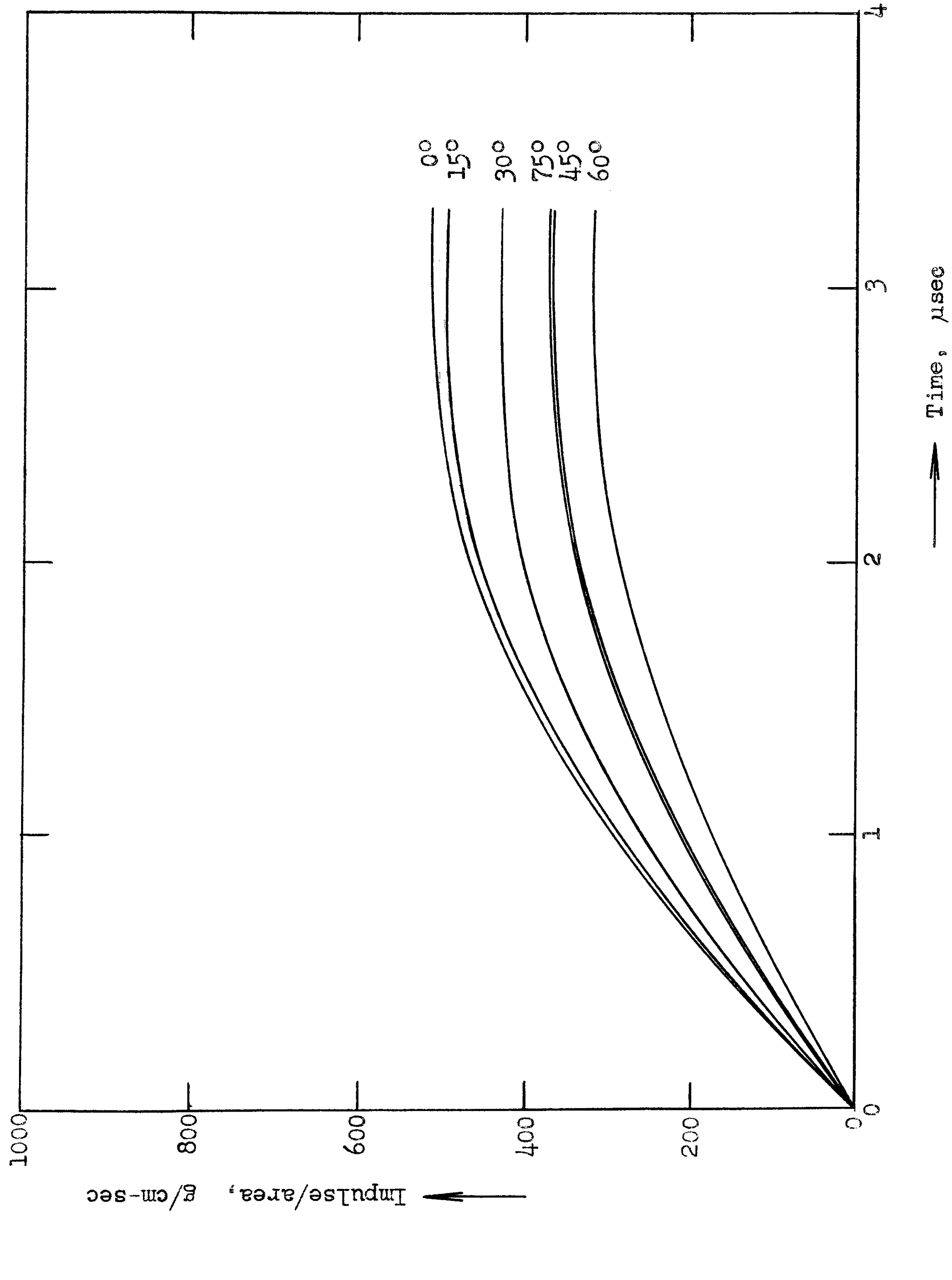

Fig. 34: Impulse per unit area vs. time, specimen J

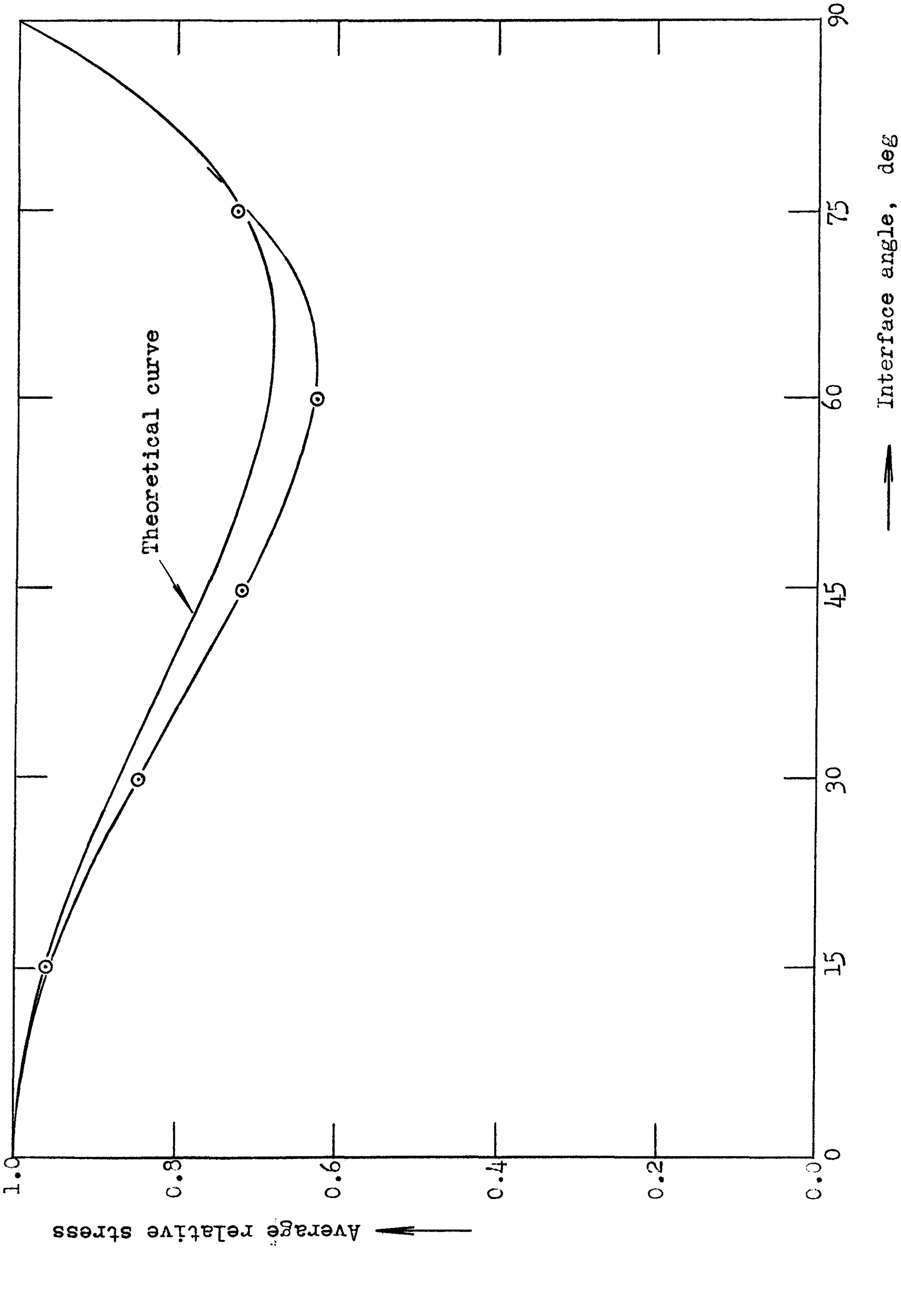

Fig. 35: Average relative stress vs. interface angle, specimen J

SUMMARY AND CONCLUSIONS

INTERFACE SERIES

The study of the effect of an oblique interface upon the transmission of stress pulses is covered by a major part of this thesis. The results of the experimental tests are shown in figs. 20, 23, 26, 29, 32, and 35, where the average relative stress transmitted across the interface is plotted against the angle of the interface: for interfaces of up to 45°, the curves follow very closely a theoretical curve; a minimum is reached between 60° and 70°, followed by a sharp rise with increasing angle of the interface. Also shown in the figures is the theoretical curve, obtained by a separate mathematical analysis. Except for specimens of the type B and C (see figs. 21 and 24), the theoretical and experimental curves seem fairly well in agreement. In tests with specimens of the type B and C, the effect of the interface angle appears to be more marked, with the minima of the experimental curves consistently lower than that of the theoretical curve. This deviation can be explained by the configuration of the particular specimens involved.

With regard to specimens of the B type, it can be seen that there are actually two oblique interfaces, both having the same angle of obliquity: one formed by the two parts of the specimen and another one between specimen and pellet. It should be expected then that the transmission factor is the second power of the transmission factor for a single interface. Therefore by taking the square root of the resulting average relative stress, we can obtain a second curve, which is fairly close to the theoretical curve (see fig. 23).

In the case of specimens of the C type, the consideration for B-type specimens does not apply. However, there are other reasons to explain the deviation from the theoretical results. In fact, it is not certain that the stress pulse radiating from the blasting cap has the same intensity and shape in all directions. It is most likely that the pulse entering normally into the specimen will be more intense than a pulse entering it obliquely. This belief is supported by the configuration of the crushing zone: rather than being spherical it is a hemi-ellipsoid, with its long axis pointing into the specimen (see also Rinehart and McClain, 1960, p. 1813).

It should be emphasized here that while theory and experiments show similar results, the mathematical analysis does not start from the same premises as the experimental work. Strictly speaking, the theoretical results apply to a plane, elastic wave (or periodic disturbance). The experiments, in turn, deal with a spherically-diverging single stress pulse, which is probably not quite elastic at the beginning. After the maximum stress decays beyond the elastic limit, the pulse will become elastic. There are, then, three differences:

Theoretical analysis	Experiments
Plane disturbance	Spherical disturbance
Periodic	Single pulse
Elastic	Elastic-Plastic

It appears that, within the limitations of the experiments, these three discordant factors do not show a substantial influence, if any.

SHAPE OF TRANSIENT PULSE

The results of this test are shown in fig. 16: Impulse per unit area vs. time, and fig. 17: Stress vs. time.

In fig. 16 the impulse per unit area increases rapidly from zero and then levels off at about 3 μsec. For $t > 5$ μsec, the impulse rises again. This new increase, rather than being a characteristic of the stress pulse itself, apparently is due to an effect of the size of the specimen. The new increase in impulse appears to coincide with a point at which the pellet thickness becomes critical -- where reflected pulses start to interfere. However, the size of the specimen does not seem to affect only the interference from pulses reflected at the sides of the specimen. If this were the case, the generated tensile stresses would tend to decrease the impulse of the pellet rather than to increase it.

It has not been the purpose of these experiments to study in detail the effect of specimen size. The conclusions which can be drawn are:

a). Specimen size affects the stress pulse -- an effect which can be substantial.

b). The effect does not seem to be of simple geometrical origin (interference of reflected pulses) but rather a distortion of the pulse shape itself.

Fig. 17 shows the shape of the stress pulse at 2 in. from the blasting cap, being propagated in a specimen of section 2 x 2 in. The pulse has a maximum stress of 445 Kg/cm^2 (6300 lb/in.^{2}) and a duration of 3 μsec.

APPENDIX I

AIR-GAP TEST

METHOD AND RESULTS

An additional test was performed to study the transmission of transient stress pulses across air gaps. Fig. 36 shows the experimental setup used in this test.

The specimen consists of a lower 1-in. Plexiglas sheet, with a 3 x 3-in. cross section. The upper part is a cube, 1 in. on a side. Four bolts keep the cube in tight connection with a set of flanges. The flanges, in turn, control the vertical movement, by which the gap width can be adjusted. A pellet located on top of the cube provides a means to measure the impulse crossing the air gap.

The prime purpose of this air-gap test was to check some of the results obtained by the conventional pellet method, particularly the total impulse per unit area of the stress pulse. By determining the shortest gap width for which no stress is transmitted into the upper section (and as a consequence, into the pellet), the impulse per unit area of the stress pulse can be determined.

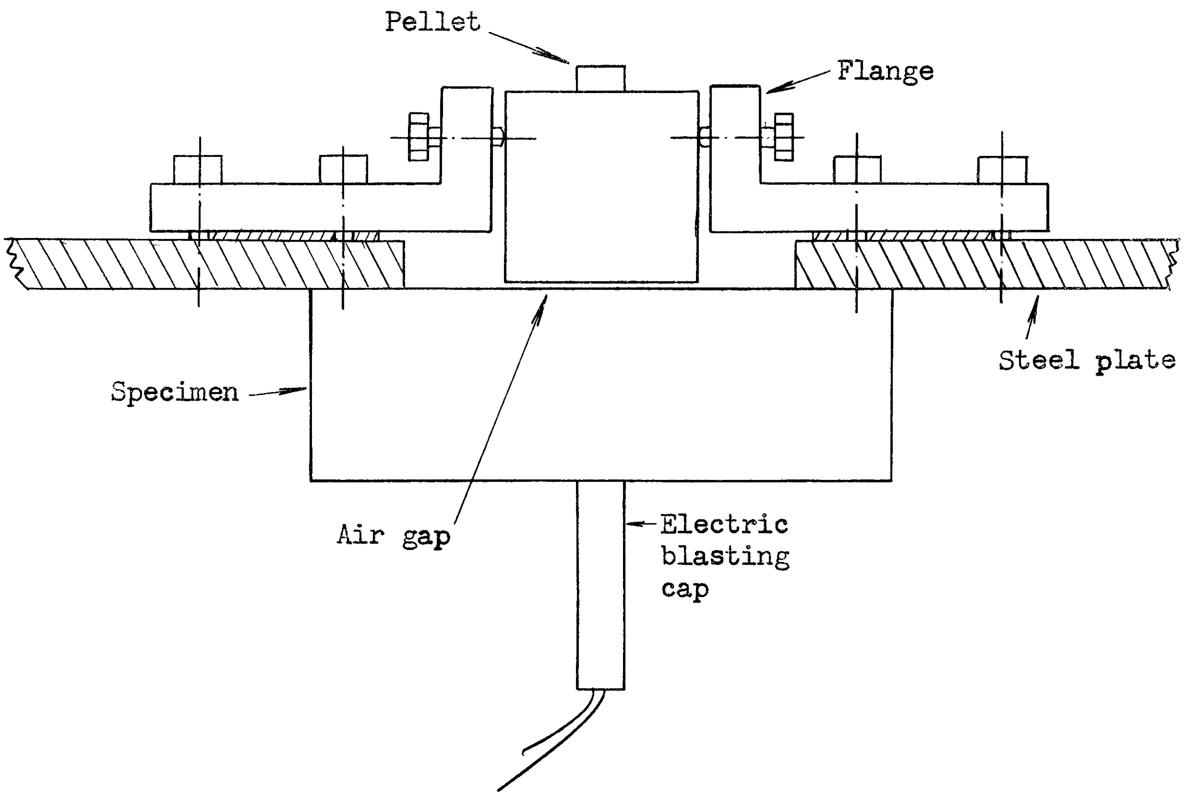

Fig. 36: Experimental setup used in air-gap test

If s_o denotes the shortest gap width with no transmission, we have

$$s_o = \int 2v \, dt$$

and with $$v = \sigma / \rho c$$

we obtain $$s_o = (2/\rho c) \int \sigma \, dt$$

or $$\int \sigma \, dt = 1/2(\rho c s_o) = I_{tot}/A$$

But this is the impulse per unit area at 1 in. from the blasting cap.

For a spherically-diverging wave, we have at 2 in.

$$\sigma_{2 \text{ in.}} = 1/2 \, \sigma_{1 \text{ in.}} \tag{43}$$

and the impulse per unit area at 2 in.:

$$I_{tot}/A = 1/4 \rho c s_o \tag{44}$$

The distance s_o was determined by increasing the gap width and measuring the velocity of the pellet. At no velocity -- with the pellet remaining in its original position -- it was assumed that the transmission of stress across the air gap was negligible. A second series was run under identical conditions, but without a film of oil between top section of specimen and pellet. This was done with the idea of obtaining s_o with higher accuracy, as the adherence of the oil may well outbalance the effect of very small impulses. Fig. 37 shows the results obtained in these two tests.

DISCUSSION

The total impulse per unit area of the stress pulse, given by eq. 44, results as 1490 g/cm-sec, taking 0.0075 in. as the shortest gap width with no transmission (s_o). The corresponding figure obtained by the pellet method is 645 g/cm-sec (fig. 16). While there is no direct explanation for the substantial difference of the two figures, the following considerations can be made:

a). the reduced size of the upper specimen section may affect the impulse transmitted into the pellet;

b). the applicability of eq. 43 (and as a consequence, of eq. 44) to an elastic-plastic stress pulse is questionable. This is based upon the fact that a plastic pulse will decay at a faster rate than an elastic pulse. This implies that the integral $\int \sigma dt$ taken at 1 in. distance from the cap is more than twice the integral at 2 in.

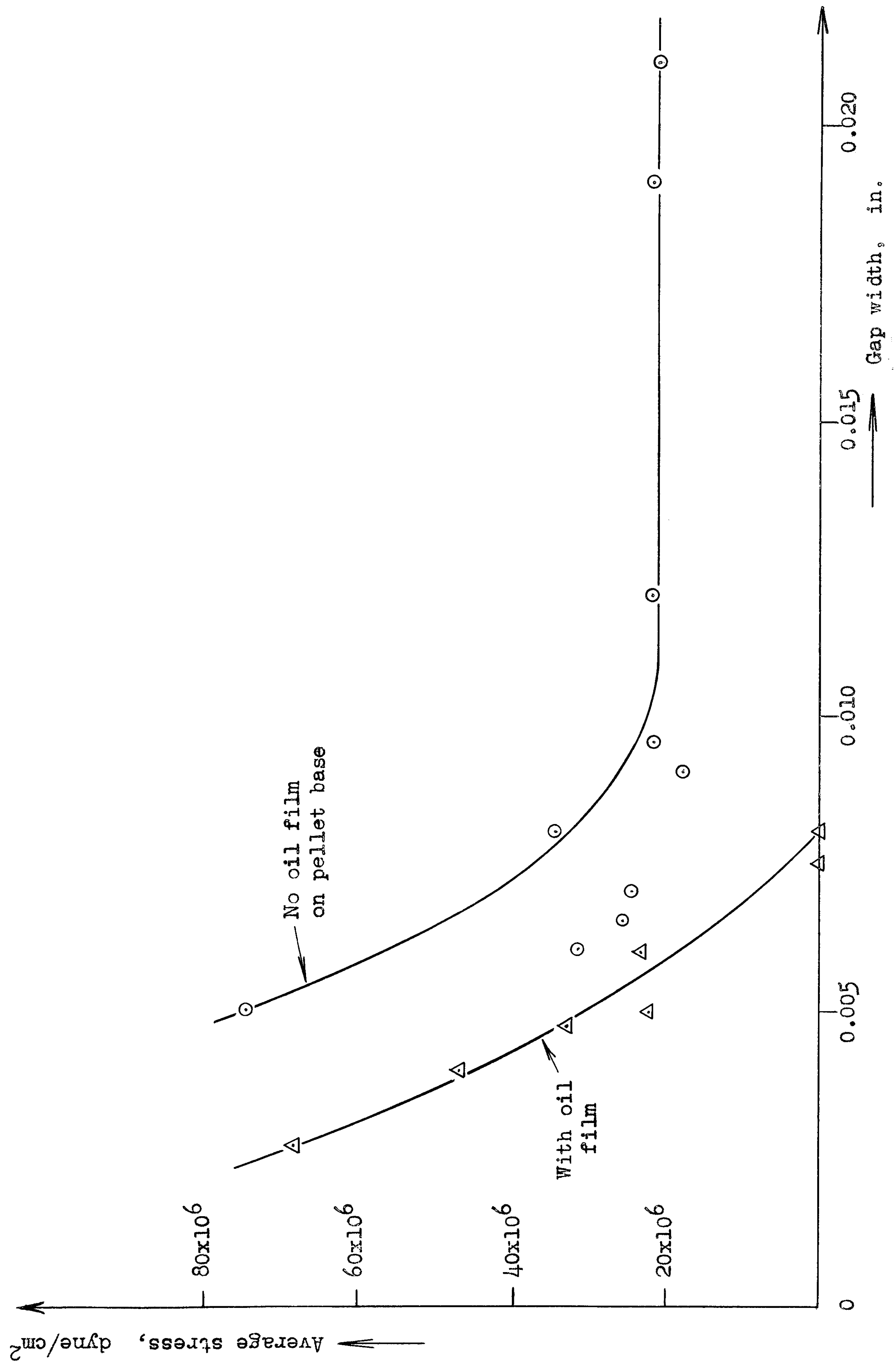

Fig. 37: Average stress transmitted across air gap vs. gap width

For gap widths of up to 0.008 in., the two curves in fig. 37 appear to be similar and separated by a constant difference. However, rather than approaching the abscissa, as should be expected, the upper curve (no oil) reaches a constant value (>0) with increasing gap width. It is assumed here that the stress transmission corresponding to the constant value does not take place across the air gap. Instead, it is quite possible that a certain impulse is transmitted through the flanges, and then reaches the pellet.

The constant vertical difference between upper and lower curves corresponds to the impulse required to outbalance the cohesive action of the oil film.

APPENDIX II

TABULAR DATA

The data obtained in the experiments are presented here in a tabular form.

The units used in these tables are the following:

Interface angle	deg
Pellet thickness	in.
Pellet speed	cm/sec
Impulse/area	g/cm-sec
Gap width	in.
Pellet section	sq in.
Average stress	dyne/cm^2

The specimen type is indicated by a capital letter, as used in figs. 18, 21, 24, 27, 30, and 33.

1. PULSE-SHAPE TEST

Specimen type	Pellet thickness	Specimen section	Pellet speed	Impulse/ area
See fig. 15	1/64	2x2	1830	86
			1900	89
			2140	100
			2450	115
			2510	118
	1/32		2450	229
			2440	228
			2220	208
			2720	255
			1960	184
	1/16		2370	444
			2370	444
			2290	429
			2370	444
			2290	429
	3/32		1929	542
			1956	550
			1911	537
	1/8		1580	592
			1678	629
			1576	590
	5/32		1473	690
			1404	658
			1455	681
	3/16		1096	616
			1192	670
			1157	650
	7/32		1052	690
			911	597
			-	-
	1/4		911	683
			960	719
			876	656
	9/32		869	732
			911	768
			736	620
	5/16		914	856
			838	785
			914	856

Specimen type	Pellet thickness	Specimen section	Pellet speed	Impulse/ area
See fig. 15	11/32	2x2	914	942
			914	942
			876	902
	3/8		914	1027
			991	1114
			991	1114
	7/16	2 1/2x2 1/2	575	754
			643	843
			643	843
	1/2	2x2	1016	1522
			1117	1674
			1151	1725
		2 1/2x2 1/2	542	812
			542	812
			508	761
	5/8	3x3	372	697
			338	633
			440	824
	1/4	2 1/2x2 1/2	866	649
			880	659
			941	705

2. INTERFACE SERIES

a). Impulse per unit area

Specimen type	Interface angle	Pellet thickness	Pellet speed	Impulse/ area
A	0	3/16	1615	908
			1538	864
			1514	851
	15		1276	717
			–	–
			1406	790
	30		992	557
			1098	617
			1120	629
	45		894	502
			715	402
			704	396
	60		860	483
			752	422
			881	495
	75		911	512
			727	408
			842	473
	0	5/32	1472	689
			1430	670
			1409	660
	15		1344	629
			1423	666
			1336	626
	30		1232	577
			990	464
			1123	526
	45		1025	480
			887	415
			893	418
	60		712	333
			752	352
			752	352
	75		–	–
			691	324
			765	358

Specimen type	Interface angle	Pellet thickness	Pellet speed	Impulse/ area
A	0	1/8	1724	646
			1584	593
			1690	633
	15		1620	607
			1665	624
			1368	512
	30		792	297
			1424	533
			1446	542
	45		1131	424
			1335	500
			905	339
	60		848	318
			856	321
			600	225
	75		899	337
			786	294
			775	290
	0	3/32	2124	597
			1837	516
			2103	591
	15		2187	614
			1568	440
			2102	590
	30		1386	389
			1446	406
			1887	530
	45		1264	355
			1370	385
			1192	335
	60		1327	373
			1432	402
			1484	417
	75		1285	361
			1120	315
			-	-

Specimen type	Interface angle	Pellet thickness	Pellet speed	Impulse/ area
A	0	1/16	2101	394
			2677	501
			2112	396
	15		2357	442
			2495	467
			–	–
	30		2056	385
			2136	400
			2195	411
	45		–	–
			1754	328
			1765	331
	60		1198	222
			1283	240
			1702	319
	75		1241	232
			1698	318
			908	170

Specimen type	Interface angle	Pellet thickness	Pellet speed	Impulse/ area
B	0	3/16	1733	974
			1766	992
			1766	992
	15		1412	794
			1412	794
			1412	794
	30		1192	670
			1179	663
			1220	686
	45		888	499
			940	528
			952	535
	60		855	480
			940	528
			875	492
	75		1489	837
			1104	620
			1464	823
	0	5/32	2022	947
			2035	953
			2003	938
	15		1733	812
			1656	776
			1573	737
	30		1343	629
			1212	568
			1296	607
	45		875	410
			1037	486
			875	410
	60		778	364
			778	364
			810	379
	75		1053	493
			1425	667
			944	442

Specimen type	Interface angle	Pellet thickness	Pellet speed	Impulse/ area
B	0	1/8	1669	625
			2375	890
			2311	866
	15		2086	782
			1842	690
			2099	786
	30		1678	629
			1556	583
			1738	651
	45		1109	416
			963	361
			1111	416
	60		785	294
			931	349
			764	286
	75		989	370
			1156	433
			963	361
	0	3/32	–	–
			–	–
			2329	654
	15		2200	618
			2394	673
			–	–
	30		1812	509
			1894	532
			1894	532
	45		1380	388
			1477	415
			1252	352
	60		963	271
			963	271
			963	271
	75		1477	415
			1380	388
			2119	595

Specimen type	Interface angle	Pellet thickness	Pellet speed	Impulse/ area
B	0	1/16	-	-
			-	-
			3351	628
	15		2700	605
			-	-
			-	-
	30		2227	417
			-	-
			2486	466
	45		1638	307
			1523	285
			1620	303
	60		1091	204
			1089	204
			1027	192
	75		1592	298
			1566	293
			835	156

Specimen type	Interface angle	Pellet thickness	Pellet speed	Impulse/ area
C	0	3/16	1250	702
			1230	691
			1190	669
	15		1150	646
			1190	669
			1250	702
	30		1190	669
			910	511
			1090	612
	45		850	478
			850	478
			760	427
	60		-	-
			540	303
			610	343
	75		750	421
			760	427
			680	382
	0	5/32	1320	618
			1390	651
			1490	698
	15		1360	637
			1390	651
			1330	623
	30		1210	567
			1090	510
			940	440
	45		900	421
			950	445
			970	454
	60		680	318
			600	281
			590	276
	75		870	407
			950	445
			840	393

Specimen type	Interface angle	Pellet thickness	Pellet speed	Impulse/ area
C	0	1/8	1610	603
			1650	618
			1520	569
	15		1590	596
			1460	547
			1520	569
	30		1370	513
			1420	532
			1290	483
	45		1030	386
			1010	378
			1080	405
	60		710	266
			710	266
			820	307
	75		1130	423
			1220	457
			860	322
	0	3/32	1920	539
			2080	584
			1980	556
	15		1890	531
			1990	559
			2020	568
	30		1720	483
			1810	508
			1710	480
	45		1060	298
			1170	329
			1390	390
	60		720	202
			820	230
			850	239
	75		1260	354
			1070	301
			1200	337

Specimen type	Interface angle	Pellet thickness	Pellet speed	Impulse/ area
C	0	1/16	-	-
			-	-
			2040	382
	15		2250	421
			2000	375
			-	-
	30		2010	376
			1910	358
			2010	376
	45		1710	320
			1590	298
			1150	215
	60		1120	210
			1020	191
			1020	191
	75		1290	242
			1350	253
			1620	303

Specimen type	Interface angle	Pellet thickness	Pellet speed	Impulse/ area
E	0	3/16	1160	652
			1220	686
			1080	607
	15		1130	635
			1020	573
			1070	601
	30		1050	590
			1060	596
			1030	579
	45		880	494
			820	461
			780	438
	60		790	444
			820	461
			840	472
	75		670	376
			540	303
			670	376
	0	5/32	1330	623
			1330	623
			1360	637
	15		1180	552
			1270	595
			1210	567
	30		980	459
			950	445
			1050	492
	45		910	426
			1000	468
			860	403
	60		860	403
			1080	506
			890	417
	75		650	304
			460	215
			810	379

Specimen type	Interface angle	Pellet thickness	Pellet speed	Impulse/ area
E	0	1/8	1460	547
			1620	607
			1590	596
	15		1420	532
			1520	569
			1020	382
	30		1140	427
			1360	510
			1380	517
	45		1100	412
			1190	446
			1170	438
	60		770	288
			930	348
			960	360
	75		-	-
			920	345
			820	307
	0	3/32	1900	534
			1780	500
			1870	525
	15		1680	472
			1740	489
			1810	508
	30		1530	430
			1350	379
			1320	371
	45		1260	354
			1190	334
			1070	301
	60		1360	382
			1430	402
			1190	334
	75		1170	329
			920	258
			1070	301

Specimen type	Interface angle	Pellet thickness	Pellet speed	Impulse/ area
E	0	1/16	2290	429
			2360	442
			2230	418
	15		2290	429
			2070	388
			2070	388
	30		2040	382
			2010	376
			2010	376
	45		1950	365
			1380	258
			1600	300
	60		1990	373
			1760	330
			1830	343
	75		1460	273
			1470	275
			1460	273

Specimen type	Interface angle	Pellet thickness	Pellet speed	Impulse/ area
F	0	1/8	1360	510
			1510	566
	15		1560	584
			1330	498
	30		1300	387
			1300	487
	45		1280	480
			1120	420
	60		1020	382
			890	333
	75		1050	393
			1180	442
	0	3/32	1630	458
			2020	568
	15		1870	525
			1780	500
	30		1780	500
			1600	450
	45		1340	376
			1450	407
	60		1140	320
			1200	337
	75		1420	399
			1520	427
	0	1/16	2130	399
			1870	350
	15		2110	395
			1990	373
	30		1810	339
			2020	378
	45		1640	307
			1820	341
	60		1760	330
			1690	316
	75		1540	288
			1570	294

Specimen type	Interface angle	Pellet thickness	Pellet speed	Impulse/area
J	0	1/8	880	330
			850	318
			1150	431
			1130	423
	15		1275	478
			1180	442
			1270	476
			1400	524
	30		-	-
			-	-
			1145	429
			860	322
	45		490	184
			1000	375
			620	232
			180	67
	60		850	318
			820	307
			630	236
			-	-
	75		620	232
			660	247
			800	300
			860	322
	0	3/32	1470	413
			1030	290
			1590	447
			-	-
	15		1280	360
			1440	405
			1610	452
			1490	419
	30		920	258
			1410	396
			1180	332
			1520	427
	45		620	174
			970	272
			950	267
			920	258

Specimen type	Interface angle	Pellet thickness	Pellet speed	Impulse/ area
J	60	3/32	1090	306
			920	258
			810	228
			930	261
	75		950	267
			1570	441
			1060	298
			1400	393
	0	1/16	1440	270
			-	-
			-	-
			-	-
	15		1505	282
			1960	367
			2120	397
			2020	378
	30		1060	198
			-	-
			-	-
			1730	324
	45		1170	219
			1200	225
			1560	292
			1120	210
	60		1240	232
			1310	245
			1110	208
			1270	238
	75		1510	283
			1830	343
			960	180
			1330	249

b). Average relative stress

Specimen type	Interface angle	Total impulse/area	Average stress	Average relative stress
A	0	678	230	1
	15	641	218	0.045
	30	550	187	0.811
	45	477	162	0.704
	60	370	128	0.546
	75	400	136	0.590
B	0	900	306	1
	15	800	272	0.889
	30	640	218	0.711
	45	478	162	0.531
	60	360	122	0.400
	75	490	166	0.544
C	0	660	224	1
	15	640	218	0.970
	30	572	194	0.867
	45	440	150	0.667
	60	315	107	0.477
	75	400	136	0.606
E	0	640	218	1
	15	590	200	0.922
	30	524	178	0.819
	45	460	156	0.719
	60	415	141	0.649
	75	390	132	0.610
F	0	510	173	1
	15	492	167	0.965
	30	432	147	0.847
	45	368	125	0.721
	60	320	109	0.627
	75	370	126	0.725
J	0	582	198	1
	15	560	190	0.963
	30	510	173	0.877
	45	460	156	0.791
	60	393	134	0.676
	75	452	154	0.777

3. AIR-GAP TEST

Pellet thickness = constant = 1/8 in.

Specimen type	Gap width	Pellet speed	Average stress	Remarks
See fig. 36	0.00275	548	68×10^6	Oil film on pellet base
	0.004	377	47×10^6	
	0.00475	268	33×10^6	
	0.005	184	23×10^6	
	0.006	192	24×10^6	
	0.0075	0	0	
	0.008	0	0	
	0.0145	0	0	
	0.005	596	74×10^6	No oil film
	0.006	254	32×10^6	
	0.0065	203	25×10^6	
	0.007	196	24×10^6	
	0.008	271	34×10^6	
	0.009	140	17×10^6	
	0.009	140	17×10^6	
	0.0095	176	22×10^6	
	0.012	175	22×10^6	
	0.019	172	21×10^6	
	0.021	167	21×10^6	

4. THEORETICAL CURVE

Interface angle	C/A	D/A	E/A	F/A
0	0.00000	0.00000	1.00000	0.00000
10	0.01548	0.17272	0.98452	0.17272
20	0.05935	0.32475	0.94065	0.32475
30	0.12420	0.43906	0.87580	0.43906
40	0.19850	0.50511	0.80150	0.50511
50	0.36748	0.52002	0.73252	0.52002
60	0.31313	0.48661	0.68687	0.48661
70	0.31208	0.40641	0.68792	0.40641
80	0.22777	0.26402	0.77223	0.26402
90	0.00000	0.00000	1.00000	0.00000

APPENDIX III

EQUIPMENT SPECIFICATIONS

PLEXIGLAS

Plexiglas is a trade name used by Rohm & Haas Co., Washington Square, Philadelphia 5, Pennsylvania. It is a thermoplastic cast acrylic resin (methyl methacrylate) with the following characteristics (at 30°C):

Tensile strength	7000 - 8000	$lb/in.^2$
Flexural strength	14,000 - 16,000	$lb/in.^2$
Compression strength	10,000 - 12,000	$lb/in.^2$
Modulus of elasticity	500,000	$lb/in.^2$
Modulus of rigidity	180,000	$lb/in.^2$
Bulk modulus	830,000	$lb/in.^2$
Refraction index	1.488 - 1.489	
Specific gravity	1.18	
Hardness Mohs	2 - 3	
Vickers	18 - 20	
Poisson's ratio	0.4	

CAMERA

A Polaroid Land Camera, Model 110A, with lens Rodenstock-Ysarex 1:4.7, f = 127 mm, was used with film Polaroid Land Picture Roll (8 pictures, 3 1/4 x 4 1/4 in.) 3000 speed, type 47. Polaroid Corporation, Cambridge 39, Massachusetts.

STROBOSCOPE

The stroboscope consists of two components:

Strobotac, type 631-BL

Range	600 - 14,500 rpm
Flash source	Internal electronic pulse generator
Flash duration	About 30 μsec

Strobolux, type 648-A

The strobolux is a slave lamp whose flashing rate must be controlled by the Strobotac. It provides 10 to 100 times more light than the Strobotac.

Flash duration	15 - 50 μsec

Both Strobotac and Strobolux are manufactured by General Radio Co., Cambridge 39, Massachusetts.

BLASTING CAPS

The same type of blasting cap was used in all tests. It was a No. 6 instantaneous loop electric blasting cap (Plas-T-Cap), produced by Olin Mathieson Chemical Corp., Explosives Division, East Alton, Illinois.

This cap has a cylindrical shape (diameter = 1/4 in., length = 1 1/8 in.) and a plastic case.

INTERFACE

Oil	Outers 445 Gun Oil		
	Outers Laboratories, Inc., Onalaska, Wisconsin		
	Density	$0.884\ g/cm^3$	
	Viscosity, absolute	12.4 centipoise	
Grease	Grease, O.D., No. 0		
	The Warren Refining & Chemical Co.,		
	Cleveland 5, Ohio		

SANDPAPER

1). TRI-M-ITE cloth discs, silicon carbide, grit 80
Minnesota Mining & Manufacturing Co.,
St. Paul 6, Minnesota

2). Behr-Manning Tufbak Durite Paper, type 280-A
Behr-Manning Co., Troy, New York

APPENDIX IV

WAVE PROPAGATION VELOCITIES IN PLEXIGLAS

The longitudinal and transverse velocities of propagation (in unbounded medium) in Plexiglas were determined by experiment. The following results were obtained:

Test No.	c_l	c_t
-	ft/sec	ft/sec
1	8650	4400
2	8630	4420
3	8730	4340
Average	8670	4387

The values used in all the calculations in this thesis are

$$c_l = 8700$$

$$c_t = 4400$$

and

$$k = 1.98$$

The technical literature indicates the following figures:

Source	Value	Method
Hughes, Pondrom, and Mims, 1949	$c_l = 8660$	Measured
	$c_t = 4160$	Measured
Hughes, Blankenship, and Mims, 1950	$c_l = 8600$	Measured
	$c_t = 4250$	Measured
Broberg, 1956, p. 35	$c_l = 8600$	Not indicated
	$c_t = 4260$	Not indicated
Gray, 1957	$c_l = 8790$	Calculated
	$c_t = 3610$	Calculated
Rinehart and Auberger, 1961	$c_l = 9090$	Measured

APPENDIX V

ACCURACY OF MEASUREMENTS

The accuracy of the velocity measurements will be considered here. There are three different effects to account for: instrumentation, drag and gravity.

a). Instrumentation - Both stroboscopes used in the tests were checked for their accuracy with an oscilloscope. The highest error found was 0.7 percent, while the error at a frequency of 6000 flashes per minute was less than 0.3 percent.

b). Drag - The effect of air drag on the pellet can be calculated. For this purpose it will be assumed that the pellet does not rotate but maintains its horizontal position while moving. We will consider the worst case: if D = force of drag, and c_D = drag coefficient, we can write

$$D = c_D \ 1/2 \rho v^2 \ A$$

in which $1/2 \rho v^2$ represents the dynamic pressure at the stagnation point. Conservation of energy requires that (neglecting compression and friction work)

$$-D \ dx = d(1/2m \ v^2)$$

or $$-c_D \, 1/2 \, \rho v^2 \, A \, dx = m \, v \, dv$$

Rearranging and integrating we obtain finally

$$v = v_o \, e^{-1/2 \, c_D \frac{\rho_{air}}{\rho_{pel}} \frac{x}{t_p}} \tag{45}$$

where v_o is initial velocity of the pellet (at $x = 0$)

t_p is thickness of pellet

and x is coordinate normal to the top of the specimen.

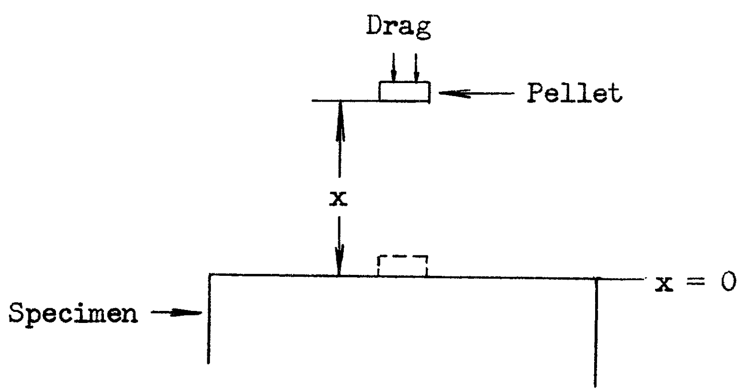

Fig. 38: Drag effect on pellet

The effect of drag is highest for thin pellets. The smallest pellet size used in standard tests was 1/16 in., and the measurements took place at $x = 1$ ft, approximately. From Marks (1951, p. 1482) we obtain for a circular disc

$$c_D = 1.11$$

We also have $\rho_{air} = 0.00105 \text{ g/cm}^3$

$$\rho_{pel} = 1.18 \text{ g/cm}^3$$

Introducing these values in eq. 45, we obtain

$$v = 0.91\ v_o$$

The measured velocity is only 91 percent of the actual initial velocity, and an error of 9 percent is involved. While this figure (9 percent) may seem high, it has to be kept in mind that this represents only the worst case: it is most unlikely that the pellet will not rotate about a horizontal axis; as a consequence, the drag effect will be strongly reduced and the error will be minimized.

c). Gravity - The effect of gravity can be also easily calculated. Conservation of energy requires that (neglecting air resistance)

$$m\ g\ x = 1/2\ m(v_o^2 - v^2)$$

Simplifying and rearranging we obtain

$$v^2 = v_o^2 - 2\ g\ x \qquad (46)$$

The effect of velocity reduction by gravity is greatest for slow pellets. Considering such a case, with $v_o = 600$ cm/sec and $x = 30$ cm, we obtain

$$v = 550 \text{ cm/sec} = 0.92\ v_o$$

Again it should be emphasized that this applies to a case in which the most adverse conditions occur simultaneously, which is unlikely to happen. With increasing pellet velocity the error decreases rapidly.

While the effects of drag and gravity act together and therefore should be combined, their maxima do not coincide but rather are diametrically opposed. In other words, for a high drag effect the gravity influence is negligible, and vice versa.

APPENDIX VI

MATHEMATICAL ANALYSIS -- EXPLANATIONS

AMPLITUDE RATIOS

Eqs. 29, 30, 31 and 32 can be written in the equivalent form

$$\begin{aligned}
\cos\alpha &= \frac{C}{A}\cos\alpha - \frac{D}{A}\sin\beta + \frac{E}{A}\cos\alpha + \frac{F}{A}\sin\beta \\
k\cos2\beta &= -\frac{C}{A}k\cos2\beta + \frac{D}{A}\sin2\beta + \frac{E}{A}k\cos2\beta + \frac{F}{A}\sin2\beta \\
\sin2\alpha &= \frac{C}{A}\sin2\alpha + \frac{D}{A}k\cos2\beta + 0 + 0 \\
0 &= 0 + 0 + \frac{E}{A}\sin2\alpha - \frac{F}{A}k\cos2\beta
\end{aligned}$$

The amplitude ratios can now be expressed as quotients of determinants:

$$\frac{C}{A} = \frac{\begin{vmatrix} \cos\alpha & -\sin\beta & \cos\alpha & \sin\beta \\ k\ \cos2\beta & \sin2\beta & k\ \cos2\beta & \sin2\beta \\ \sin2\alpha & k\ \cos2\beta & 0 & 0 \\ 0 & 0 & \sin2\alpha & -k\ \cos2\beta \end{vmatrix}}{\begin{vmatrix} \cos\alpha & -\sin\beta & \cos\alpha & \sin\beta \\ -k\ \cos2\beta & \sin2\beta & k\ \cos2\beta & \sin2\beta \\ \sin2\alpha & k\ \cos2\beta & 0 & 0 \\ 0 & 0 & \sin2\alpha & -k\ \cos2\beta \end{vmatrix}} = \frac{|C|}{|A|}$$

$$\frac{D}{A} = \frac{\begin{vmatrix} \cos\alpha & \cos\alpha & \cos\alpha & \sin\beta \\ -k\ \cos2\beta & k\ \cos2\beta & k\ \cos2\beta & \sin2\beta \\ \sin2\alpha & \sin2\alpha & 0 & 0 \\ 0 & 0 & \sin2\alpha & -k\ \cos2\beta \end{vmatrix}}{\begin{vmatrix} \cos\alpha & -\sin\beta & \cos\alpha & \sin\beta \\ -k\ \cos2\beta & \sin2\beta & k\ \cos2\beta & \sin2\beta \\ \sin2\alpha & k\ \cos2\beta & 0 & 0 \\ 0 & 0 & \sin2\alpha & -k\ \cos2\beta \end{vmatrix}} = \frac{|D|}{|A|}$$

$$\frac{E}{A} = \frac{\begin{vmatrix} \cos\alpha & -\sin\beta & \cos\alpha & \sin\beta \\ -k\cos2\beta & \sin2\beta & k\cos2\beta & \sin2\beta \\ \sin2\alpha & k\cos2\beta & \sin2\alpha & 0 \\ 0 & 0 & 0 & -k\cos2\beta \end{vmatrix}}{\begin{vmatrix} \cos\alpha & -\sin\beta & \cos\alpha & \sin\beta \\ -k\cos2\beta & \sin2\beta & k\cos2\beta & \sin2\beta \\ \sin2\alpha & k\cos2\beta & 0 & 0 \\ 0 & 0 & \sin2\alpha & -k\cos2\beta \end{vmatrix}} = \frac{|E|}{|A|}$$

$$\frac{F}{A} = \frac{\begin{vmatrix} \cos\alpha & -\sin\beta & \cos\alpha & \cos\alpha \\ -k\cos2\beta & \sin2\beta & k\cos2\beta & k\cos2\beta \\ \sin2\alpha & k\cos2\beta & 0 & \sin2\alpha \\ 0 & 0 & \sin2\alpha & 0 \end{vmatrix}}{\begin{vmatrix} \cos\alpha & -\sin\beta & \cos\alpha & \sin\beta \\ -k\cos2\beta & \sin2\beta & k\cos2\beta & \sin2\beta \\ \sin2\alpha & k\cos2\beta & 0 & 0 \\ 0 & 0 & \sin2\alpha & -k\cos2\beta \end{vmatrix}} = \frac{|F|}{|A|}$$

Solving the determinants, with the notation used at the extreme right in equations on p. 106-107, we obtain

$$|A| = 2\cos\alpha\,(k\cos2\beta + 2\sin\alpha\sin\beta)(k^2\cos^2 2\beta + \sin2\alpha\sin2\beta)$$

$$|C| = 2\cos\alpha\,(k\cos2\beta + 2\sin\alpha\sin\beta)(\sin2\alpha\sin2\beta)$$

$$|D| = 2\cos\alpha\,(k\cos2\beta + 2\sin\alpha\sin\beta)(k\cos2\beta\sin2\alpha)$$

$$|E| = 2\cos\alpha\,(k\cos2\beta + 2\sin\alpha\sin\beta)(k^2\cos^2 2\beta)$$

$$|F| = 2\cos\alpha\,(k\cos2\beta + 2\sin\alpha\sin\beta)(k\cos2\beta\sin2\alpha)$$

which for the amplitude ratios results as

$$\frac{C}{A} = \frac{\sin2\alpha\ \sin2\beta}{k^2\ \cos^2 2\beta + \sin2\alpha\ \sin2\beta}$$

$$\frac{D}{A} = \frac{k\ \cos2\beta\ \sin2\alpha}{k^2\ \cos^2 2\beta + \sin2\alpha\ \sin2\beta}$$

$$\frac{E}{A} = \frac{k^2\ \cos^2 2\beta}{k^2\ \cos^2 2\beta + \sin2\alpha\ \sin2\beta}$$

$$\frac{F}{A} = \frac{k\ \cos2\beta\ \sin2\alpha}{k^2\ \cos^2 2\beta + \sin2\alpha\sin2\beta}$$

as in eqs. 33 to 36 on p. 25-26.

CONSERVATION OF ENERGY

The energy per unit area of interface and per period is given by

$$H = K^2\,\frac{\pi^2\rho\ c}{T\ \sin\gamma}\,\sin2\gamma$$

where K is displacement amplitude

γ is respective angle of incidence, reflection or refraction.

Conservation of energy requires that

$$H_A = H_C + H_D + H_E + H_F$$

in the case of an incident longitudinal wave. Omitting the common terms π^2, ρ and T, which can be divided out, we have

$$\frac{A^2\ c_l \sin 2\alpha}{\sin\alpha} = \frac{C^2\ c_l \sin 2\alpha}{\sin\alpha} + \frac{D^2\ c_t \sin 2\beta}{\sin\beta} + \frac{E^2\ c_l \sin 2\alpha}{\sin\alpha} + \frac{F^2\ c_t \sin 2\beta}{\sin\beta}$$

But

$$\frac{c_l}{\sin\alpha} = \frac{c_t}{\sin\beta}$$

and dividing also by $A^2 \sin 2\alpha$:

$$1 = \frac{C^2}{A^2} + \frac{D^2}{A^2}\frac{\sin 2\beta}{\sin 2\alpha} + \frac{E^2}{A^2} + \frac{F^2}{A^2}\frac{\sin 2\beta}{\sin 2\alpha}$$

which is Blut's check equation of energy.

Introducing the amplitude ratios in Blut's equation,

$$1 = \frac{1}{(k^2\ \cos^2 2\beta + \sin 2\alpha \sin 2\beta)^2}\ (\sin^2 2\alpha \sin^2 2\beta + k^2 \cos^2 2\beta \sin 2\alpha \sin 2\beta + k^4 \cos^4 2\beta + k^2 \cos^2 2\beta \sin 2\alpha \sin 2\beta)$$

or 1 = 1, which proves that energy is conserved.

MAXIMA AND MINIMA OF AMPLITUDE RATIOS

By taking the derivative of the equations of amplitude ratio vs. interface angle, their maxima (or minima) and slopes at 0° and 90° have been determined.

		Maxima/Minima	Slope at 0°	Slope at 90°
Reflected long. wave	(C/A)	Max. at ≈ 65°	0	-1.85
Reflected trans. wave	(D/A)	Max. at ≈ 45°	1.01	-2.06
Transmitted long. wave	(E/A)	Min. at ≈ 65°	0	1.85
Transmitted trans. wave	(F/A)	Max. at ≈ 45°	1.01	-2.06

BOUNDARY CONDITIONS

The mathematical transformations required to obtain eqs. 29 to 32 (p. 25) are schematized here.

Eq. 29 - It is only a matter of inspection to visualize how this equation is obtained. It results as the combination of eqs. 17 and 27a to 27e.

Eq. 30 - The mathematical transformation will be performed for one term of eq. 30, this procedure being common to all other terms.

For the incident wave we have

$$u_A = \phi_A \cos\alpha = A\, e^{i\, p(t - \frac{y \sin\alpha + x \cos\alpha}{c_1})} \cos\alpha$$

$$v_A = \phi_A \sin\alpha = A\, e^{i\, p(t - \frac{y \sin\alpha + x \cos\alpha}{c_1})} \sin\alpha$$

Using eq. 24 we can express eq. 18 in the form

$$\sigma_{xx} = \lambda\theta + 2\mu \frac{\partial u}{\partial x} = (\lambda + 2\mu)\frac{\partial u}{\partial x} + \frac{\partial v}{\partial y}$$

which can be transformed into

$$(\sigma_{xx})_A = - A\, p\, \rho\, c_1\, e^{i\, p\, (t - \frac{y \sin\alpha + x \cos\alpha}{c_1})} \cos 2\beta$$

with the aid of eqs. 22 and 23.

At the boundary, $x = 0$ and y is common to all terms; whence, the exponential function and also p and ρ may be divided out of each term.
Eqs. 31 and 32 - These equations are obtained from the boundary conditions 19a and 20a, respectively.

From eq. 25

$$\sigma_{xy} = \mu \left(\frac{\partial v}{\partial x} + \frac{\partial u}{\partial y}\right)$$

where $$\frac{\partial v}{\partial x} = -A\ p\ e^{i\ p\ \left(t - \frac{y \sin\alpha + x \cos\alpha}{c_1}\right)} \frac{\sin\alpha \cos\alpha}{c_1}$$

and $$\frac{\partial u}{\partial y} = -A\ p\ e^{i\ p\ \left(t - \frac{y \sin\alpha + x \cos\alpha}{c_1}\right)} \frac{\sin\alpha \cos\alpha}{c_1}$$

We then obtain

$$(\sigma_{xy})_A = -\frac{1}{c_1} \mu\ A\ p\ e^{i\ p\ \left(t - \frac{y \sin\alpha + x \cos\alpha}{c_1}\right)} \sin 2\alpha$$

where again μ, p and the exponential function can be divided out. Amplifying by $(c_1\ c_t)$ we obtain the terms as shown in eqs. 31 and 32.

BIBLIOGRAPHY

Blut, Heinrich, 1932, Ein Beitrag zur Theorie der Reflexion und Brechung elastischer Wellen an Unstetigkeitsflächen: Zeitschrift für Geophysik, v. 8, p. 130-144.

Broberg, K. B., 1956, Shock waves in elastic and elastic-plastic media: Stockholm, 141 p.

Cagniard, L., 1939, Reflexion et refraction des ondes seismiques progressives: Paris, Gauthier-Villars, 255 p.

Duvall, Wilbur I., 1953, Strain-wave shapes in rock near explosions: Geophysics, v. 18, no. 2, p. 310-323.

Duvall, Wilbur I., and Atchison, Thomas C., 1950, Vibrations associated with a spherical cavity in an elastic medium: U.S. Bur. Mines Rept. Inv. 4692, 9 p.

Gray, D. E., 1957, American Institute of Physics handbook: New York, McGraw-Hill, p. 3-80.

Hodgman, Charles D., 1958, Handbook of chemistry and physics: Cleveland, Chemical Rubber Publishing Co.

Hughes, D. S., Blankenship, E. B., and Mims, R. L., 1950, Variation of elastic moduli and wave velocity with pressure and temperature in plastics: Jour. Appl. Physics, v. 21, no. 4, p. 294-297.

Hughes, D. S., Pondrom, W. L., and Mims, R. L., 1949, Transmission of elastic pulses in metal rods: Phys. Rev., v. 75, no. 10, p. 1552-1556.

Ito, Ichiro, Terada, Makoto, and Sakurai, Takehisa, 1960, Stress waves in rocks and their effects on rock breakage: Memoirs of the Faculty of Engineering, Kyoto University, v. 22, pt. 1, 17 p.

Kolsky, H., 1953, Stress waves in solids: Oxford, Clarendon Press, 211 p.

Love, A. E. H., 1934, A treatise on the mathematical theory of elasticity: Cambridge University Press, 643 p.

Macelwane, J. B., 1936, Introduction to theoretical seismology, part I, geodynamics: New York, John Wiley, 366 p.

Marks, Lionel S., 1951, Mechanical engineer's handbook: New York, McGraw-Hill.

Morris, George, 1950, Some considerations of the mechanism of the generation of seismic waves by explosives: Geophysics, v. 15, no. 1, p. 61-69.

Nunley, C. D., 1960, Transmission of plane elastic waves through layered media: Thesis, Dept. of Geophysics, Graduate School, University of Tulsa, 43 p.

Poncelet, E. F., 1957, Propagation and reflection of waves in sheets and plates: Stanford Research Institute, Poulter Laboratories, Lab. Tech. Report 007-57, 30 p.

Rinehart, John S., 1951, Some quantitative data bearing on the scabbing of metals under explosive attack: Jour. Appl. Physics, v. 22, no. 5, p. 555-560.

_____, 1960, On fractures caused by explosions and impacts: Colorado School of Mines Quarterly, v. 55, no. 4, 155 p.

Rinehart, John S., and Auberger, Michel, 1961, Ultrasonic attenuation of longitudinal waves in plastics: Jour. Appl. Physics, v. 32, no. 2, p. 219-222.

Rinehart, John S., and McClain, William, 1960, Experimental determination of stresses generated by an electric detonator: Jour. Appl. Physics, v. 31, no. 10, p. 1809-1813.

Rinehart, John S., and Pearson, John, 1954, Behavior of metals under impulsive loads: Cleveland, American Society for Metals, 236 p.

Selberg, H. L., 1952, Transient compression waves from spherical and cylindrical cavities: Arkiv för Fysik, Stockholm, v. 5, no. 7, p. 97-108.

Simonds, H. R., and Ellis, C., 1943, Handbook of plastics: D. van Nostrand, p. 154.